Journal of Magnetic Resonance 206 (2010) 227–240

Contents lists available at ScienceDirect

Journal of Magnetic Resonance

journal homepage: www.elsevier.com/locate/jmr

Exact solution to the Bloch equations and application to the Hahn echo

Alex D. Bain [a,*], Christopher Kumar Anand [b], Zhenghua Nie [c]

[a] Department of Chemistry and Chemical Biology, McMaster University, 1280 Main St. W., Hamilton, Ontario, Canada L8S 4M1
[b] Department of Computing and Software, McMaster University, 1280 Main St. W., Hamilton, Ontario, Canada L8S 4M1
[c] School of Computational Engineering and Science, McMaster University, 1280 Main St. W., Hamilton, Ontario, Canada L8S 4M1

ARTICLE INFO

Article history:
Received 23 June 2010
Revised 16 July 2010
Available online 7 August 2010

Keywords:
Bloch Equations
Lagrange interpolation
Projection operators
Hahn Echo
Measurements of transverse relaxations
Rectangular pulses
Fitting models

ABSTRACT

The exact symbolic solution of the Bloch equations is given in the Lagrange form and illustrated with R_2 experiments using a Hahn echo. Two different methods are also applied to approximately solve the Bloch equations, we find that splittings with effective-field interpretations are very substantially better than other approximations by comparing the errors. Estimates of transverse relaxation, R_2, from Hahn echos are effected by frequency offset and field inhomogeneity. We use exact solutions of the Bloch equations and simulations to quantify both effects, and find that even in the presence of expected B_0 inhomogeneity, off-resonance effects can be removed from R_2 measurements, when $\|\omega\| \leqslant 0.5\gamma B_1$, by fitting the exact solutions of the Bloch equations. Further, the experiments and simulations show that the fitting models with the exact solutions of the Bloch equations do not depend on the sampling density and delay times.

1. Introduction

Pulse sequences are the core of modern NMR. These consist of bursts of radiofrequency (rf) irradiation (pulses) followed by periods of free evolution (delays) [1–3]. Sophisticated combinations of these manipulations allow us to extract almost all possible information about a spin system. For most spin systems, the static energy levels are well-understood, so it is their evolution in time during a pulse sequence that most interests us. In order for us to understand current experiments and design new ones, we need accurate theoretical descriptions of the dynamics of a spin system. The projection operator formalism has been applied to treat motion in quantum mechanics by Löwdin [4], and some solutions of the density matrix evolution in closed analytical form have been expressed in the polynomial expressions of exponential operators using the projection operator formalism [5]. In this paper we concentrate on the simplest example, the spin-$\frac{1}{2}$ system and provide a full and exact solution. This system is described by the well-known Bloch equations, which contain the effects of precession, rf irradiation and relaxation [6–10]. Under some simplifying approximations, solutions to these equations are well-known, but the full and exact solution is not trivial [11–15]. We apply some methodology to work on the matrix form to provide a solution which is more in keeping with current theory, and which can easily be extended to more complex systems as the projection operator formalism does [5].

The paper is organized as the following. The Section (1) discusses the challenges of symbolically solving the Bloch equations, particularly, by the eigen-decomposition method. The Section (2) gives the full algebraic solution of the Bloch equations using the Lagrange interpolation. This method can avoid the problem in computing the inverse of eigenvectors which is discussed in this section. The explicit solution of the Bloch equations is still unwieldy, we present two ways to approximate the solution of the Bloch equations in Section (3) including approximate eigenvalues and split-operator methods. Because the operator splittings are not unique, we show that splittings with effective-field rotations are better than other approximations by comparing the errors. Then we illustrate the computation of the Hahn echo by applying these exact and approximate solutions of the Bloch equations in Section (4). At last, we demonstrate improvements of measured R_2 by applying the exact solution of the Bloch equations to fit the experiments of the Hahn echo in Section (5). The appendixes show the theorems we apply in this paper, solutions of free evolution, the special case $R_1 = R_2$ of the Bloch equations, and some results of calculations of the Hahn echo.

The most powerful approximation in spin dynamics is to ignore relaxation, or at least to restrict it to operating only during delays. This is slightly stronger than the common assumption of *hard* pulses. An rf pulse is hard if the rf terms dominate all other interactions, such as off-resonance effects and relaxation. With this

* Corresponding author. Fax: +1 (905) 522 2509.
E-mail address: bain@mcmaster.ca (A.D. Bain).

1090-7807/$ - see front matter © 2010 Elsevier Inc. All rights reserved.
doi:10.1016/j.jmr.2010.07.012

approximation, a pulse becomes equivalent to a rotation of the frame of reference, whose effect is relatively easy to calculate. In the standard product operator formalism [16,17], this is done by exploiting the simple commutator rules for a spin-$\frac{1}{2}$. This hard pulse approximation implies the pulse is instantaneous, so there is no time for evolution or relaxation to occur. With these approximations we can understand the vast majority of pulse NMR experiments.

Significant discrepancies arise, however, when numerically simulating experiments involving modern high-field magnets and cold probes. In high-field magnets offset effects can be significant, since the evolution frequencies at the edges of a spectrum can be comparable to the rf magnetic field in frequency units. Modern cold probes give excellent sensitivity, but are often restricted in the peak power they will tolerate. Relaxation, in normal practice, can safely be ignored during a single pulse, since the pulse durations are tens of microseconds. However, many dynamic experiments rely on measurements of R_2, either by $R_{1\rho}$ or by CPMG methods. In these cases, significant relaxation may occur during the total time the rf is on [18,19]. In order to deal with these imperfections, a number of approaches are available.

If the pulse is relatively long and weak, but relaxation can be ignored, then the behaviour of a single line is well-described by rotation about an effective magnetic field which is not in the xy plane [20–23]. If we use this as our mathematical model, then a slightly more complicated analysis of a simple experiment will work. Alternatively, we can design more sophisticated composite or shaped pulses which compensate for off-resonance effects [24–29]. In this case, a more complicated experiment will lead to a simpler analysis of the data. In this work, we study the former case, with the simple experiment and the complicated analysis.

We restrict the calculation to a single line NMR spectrum, without any time-dependent terms in the Hamiltonian. The full description in this case is given by the Bloch equations (Eq. (1)) [7]. These equations contain a number of terms to describe the evolution and relaxation of the spin system itself and to describe the interaction with the rf field. The solution we offer here must be equivalent to the Laplace transform solution [11], since both are exact. This newer solution is phrased in terms of propagators and explicit time dependence. In this way, it fits in with the common ways of working with pulse sequences. Moreover, the method is entirely general and can be extended to larger systems.

$$\frac{dM_x}{dt} = -\omega M_y + \gamma B_1 \sin\phi M_z - \frac{1}{T_2} M_x \tag{1a}$$

$$\frac{dM_y}{dt} = \omega M_x - \gamma B_1 \cos\phi M_z - \frac{1}{T_2} M_y \tag{1b}$$

$$\frac{dM_z}{dt} = -\gamma B_1 \sin\phi M_x + \gamma B_1 \cos\phi M_y - \frac{1}{T_1}(M_z - 1) \tag{1c}$$

In these equations, where ω is the resonance offset, γ is the gyromagnetic ratio, B_1 is the strength of the rf pulse (we suppose $\gamma B_1 \geqslant 0$ in this paper), ϕ is the phase of the rf field with respect to the x axis, T_1 is the longitudinal relaxation time, and T_2 is the transverse relaxation time.

There are a number of familiar solutions to these equations in special cases. The first one is the steady-state solution, which was needed to explain continuous-wave NMR. The time derivatives are set to zero and we solve for the steady-state magnetizations [9,30]. In pulsed NMR, if we have free precession (the rf term is zero), then the x and y magnetizations oscillate at the Larmor frequency and relax at a rate of $1/T_2$ and the z magnetization relaxes back to its non-zero equilibrium value with a rate of $1/T_1$. If we have a long T_1, the change in the z magnetization is small. We can often treat the spin–lattice relaxation such that the z magnetization relaxes to zero, rather than a non-zero value, further simplifying the calculations. Under these conditions, we are solving a set of 3×3 matrix equations.

In order to treat the z magnetizations properly, we first convert the Bloch equations to a homogeneous form [31,32]:

$$\frac{d}{dt}\begin{pmatrix} M_x \\ M_y \\ M_z \\ M_e \end{pmatrix} = \begin{pmatrix} -\frac{1}{T_2} & -\omega & \gamma B_1 \sin\phi & 0 \\ \omega & -\frac{1}{T_2} & -\gamma B_1 \cos\phi & 0 \\ -\gamma B_1 \sin\phi & \gamma B_1 \cos\phi & -\frac{1}{T_1} & \frac{1}{T_1} \\ 0 & 0 & 0 & 0 \end{pmatrix} \begin{pmatrix} M_x \\ M_y \\ M_z \\ M_e \end{pmatrix} \tag{2}$$

where M_e is the equilibrium z magnetization which can be set as a constant number 1. In order to simplify the notations, in the following sections, we define $b_1 \equiv \gamma B_1$, $R_1 \equiv \frac{1}{T_1}$, $R_2 \equiv \frac{1}{T_2}$, $\mathbf{A}$ to be the coefficient matrix and $\mathbf{M}$ the vector $(M_x, M_y, M_z, M_e)^T$, where T means transpose. The matrix $\mathbf{A}$ can be seen as a sum of three matrices which respectively represent the Larmor precession ($\boldsymbol{\Omega}$), the rf field ($\boldsymbol{\gamma}\mathbf{B_1}$) and the relaxation ($\mathbf{R}$),

$$\mathbf{A} = \boldsymbol{\Omega} + \boldsymbol{\gamma}\mathbf{B_1} + \mathbf{R} \tag{3}$$

with

$$\boldsymbol{\Omega} \equiv \begin{pmatrix} 0 & -\omega & 0 & 0 \\ \omega & 0 & 0 & 0 \\ 0 & 0 & 0 & 0 \\ 0 & 0 & 0 & 0 \end{pmatrix} \tag{4a}$$

$$\boldsymbol{\gamma}\mathbf{B_1} \equiv \begin{pmatrix} 0 & 0 & b_1 \sin\phi & 0 \\ 0 & 0 & -b_1 \cos\phi & 0 \\ -b_1 \sin\phi & b_1 \cos\phi & 0 & 0 \\ 0 & 0 & 0 & 0 \end{pmatrix} \tag{4b}$$

$$\mathbf{R} \equiv \begin{pmatrix} -R_2 & 0 & 0 & 0 \\ 0 & -R_2 & 0 & 0 \\ 0 & 0 & -R_1 & R_1 \\ 0 & 0 & 0 & 0 \end{pmatrix} \tag{4c}$$

Then the Bloch equations can be written as

$$\frac{d\mathbf{M}(\mathbf{t})}{dt} = \mathbf{A} \cdot \mathbf{M}(t) \tag{5}$$

These equations form a system of first-order differential equations, so if the matrix $\mathbf{A}$ is constant in a time interval, they have an analytical solution in terms of the exponential of the matrix with the given initial states [33–37],

$$\mathbf{M}(t) = e^{\mathbf{A}t}\mathbf{M}(0) \tag{6}$$

For simple cases it is straightforward to compute a symbolic solution, but the full case offers some challenges. A standard and general way of calculating a matrix exponential is to first obtain the eigenvalues and eigenvectors of the matrix,

$$\mathbf{A} = \mathbf{U}\boldsymbol{\Lambda}\mathbf{U}^{-1} \tag{7}$$

where $\boldsymbol{\Lambda}$ is a diagonal matrix which represents the eigenvalues and the jth column of $\mathbf{U}$ is the vector of eigenvectors corresponding to the jth diagonal element of $\boldsymbol{\Lambda}$. The matrix of eigenvectors of the original matrix also diagonalizes the exponential of the matrix,

$$e^{\mathbf{A}t} = \mathbf{U}e^{\Lambda t}\mathbf{U}^{-1} \tag{8}$$

Provided the original matrix is Hermitian, this is simple because the inverse of the matrix $\mathbf{U}$ is the conjugate transpose of the matrix $\mathbf{U}$. Relaxation (which destroys the Hermitian character) can be approximated afterwards, provided the terms are small.

The full homogeneous Bloch equations are not Hermitian. This means that both the eigenvalues and eigenvectors may be complex numbers. For the eigenvalues, this is clearly appropriate, since the

imaginary part of the exponential gives the oscillation and the real part gives the decay. A similar situation occurs in chemical exchange calculations [38–40]. The exact eigenvalues are relatively simple to obtain. They are the roots of the characteristic polynomial associated with the matrix **A**, which is

$$\begin{aligned} p_{\mathbf{A}}(\lambda) &= det(\mathbf{A}-\lambda\mathbf{I}) \\ &= \left(\lambda^3 + (R_1+2R_2)\lambda^2 + (\omega^2 + b_1^2 + (2R_1+R_2)R_2)\lambda \right. \\ &\quad \left. + \left(b_1^2R_2 + \omega^2R_1 + R_1R_2^2\right)\right)\lambda \end{aligned} \tag{9}$$

Clearly, one eigenvalue is zero, and the other three eigenvalues are the roots of the cubic polynomial which is the same as Eq. (12) of [12] and Eq. (21) of [14]. The formula for the roots of a cubic polynomial is not trivial, but is readily available [41]. [12,14] also give the roots of this specific cubic polynomial. In our computation, the eigenvalues of the matrix **A** are directly given by the Maple[1] function *Eigenvalues* which are the same as solving $p_{\mathbf{A}}(\lambda) = 0$ by the Maple function *solve*. If relaxation dominates and the spin is on-resonance, the cubic polynomial has three real roots, but the more common case, when $(R_1 - R_2)^2 < 4b_1^2$ (the quadratic term in the cubic is small), the cubic polynomial has one real root and two other conjugate complex roots. In the simplest case, the real root is $-R_1$ and the two complex roots are the two counter-rotating *xy* magnetizations which relax as $-R_2$. A more complete discussion of the roots of a general cubic polynomial can be found in [41].

To complete the calculation Eq. (8), we also need the eigenvectors. This is more difficult, since not only are the eigenvectors complex-valued, but there is a distinction between left and right eigenvectors [42]. For the Hermitian case, the inverse of the transformation defined by the eigenvectors is just its adjoint, the complex conjugate transpose. For the non-Hermitian Bloch equations, we must calculate the inverse explicitly. A computer algebra program such as Maple can calculate the roots symbolically and the eigenvectors. The inverse can be computed, but the expressions are unmanageable. A different approach to the matrix exponential is needed.

In the next section, we will show that for these four equations, the exponential can be exactly expressed as a sum of four products of matrices—no inverses are needed. We still need the eigenvalues, but they are available from the characteristic polynomial (Eq. (9)). This combination gives us an exact symbolic solution of the full set of Bloch equations, including all the terms.

2. The exact symbolic solution of the Bloch equations

We concentrate on the generalized Bloch equations with all terms, which is equivalent to including evolution and relaxation in a pulse. A hard pulse assumes that the offset and relaxation rates are ignored in the Bloch equations which means $\boldsymbol{\Omega}$ and **R** are set to **0**. This assumption makes the matrix **A** of a hard pulse equivalent to an infinitesimal rotation. Its symbolic exponential is therefore a full rotation matrix. When the evolution is free, we delete the rf terms in the matrix **A** (setting $\gamma\mathbf{B_1}$ to be **0**) and the exponential of the matrix **A** is easily calculated, particularly if the relaxation terms are small. In this subsection, we will concentrate on computing the exact symbolic solution of $e^{\mathbf{A}t}$, where **A** has all of these terms.

Formally, the exponential of a matrix can be defined as its convergent Taylor series [34,36], but this is a poor method of calculation. Moler and van Loan discuss a number of better approaches, including approximation theory, eigen decompositions, differential equations, and the matrix characteristic polynomial to compute the exponential of a matrix [34], but not all of them can be applied to compute a symbolic solution of the exponential of a matrix in general, and the usefulness of the solution varies. For example, the eigen-decomposition method which was used to compute the symbolic exponential of a 16-by-16 Liouvillian matrix for evaluating the spin echo of a coupled-spin system [43], can be applied to solve the Bloch equations symbolically, but the solution is unmanageably large. Although the dimension of the matrix is only 4-by-4 its non-Hermitian character makes the left- and right-eigenvectors much more complicated, for example, the result of Maple's *MatrixExponential* is 11.2 Megabytes.

Instead of working with the eigen decomposition, we apply the Lagrange interpolation method [37] which can be seen as applying the projection operator formalism to compute an exponential in the matrix form [4,5]. For a finite matrix, this gives an exact expression of the matrix exponential, but only the eigenvalues are needed. These are more accessible since they are roots of the matrix characteristic polynomial as Eq. (9).

The vector of the eigenvalues of the matrix **A** which are obtained by solving the equation $p_{\mathbf{A}}(\lambda) = 0$ (Eq. (9)) is

$$\boldsymbol{\lambda} = \begin{bmatrix} \lambda_1 \\ \lambda_2 \\ \lambda_3 \\ \lambda_4 \end{bmatrix} \tag{10}$$

and

$$\lambda_1 = E_1/6 - 6\frac{E_2}{E_1} - 1/3R_1 - 2/3R_2 \tag{11a}$$

$$\lambda_2 = u_2 + iu_3 \tag{11b}$$

$$\lambda_3 = u_2 - iu_3 \tag{11c}$$

$$\lambda_4 = 0 \tag{11d}$$

in which

$$E_1 = \left(-8(R_1-R_2)(9\omega^2 + (R_1-R_2)^2) + 36(R_1-R_2)b_1^2 + 12\sqrt{E_3}\right)^{1/3} \tag{12a}$$

$$E_2 = \frac{1}{3}\left(\omega^2 + b_1^2\right) - \frac{1}{9}(R_1-R_2)^2 \tag{12b}$$

$$\begin{aligned} E_3 &= 12\left(b_1^2+\omega^2\right)^3 + 24(R_1-R_2)^2\left(\omega^2 - \frac{5+3\sqrt{3}}{4}b_1^2\right) \\ &\quad \times \left(\omega^2 - \frac{5-3\sqrt{3}}{4}b_1^2\right) + 12(R_1-R_2)^4\omega^2 \end{aligned} \tag{12c}$$

$$u_2 = -\frac{E_1}{12} + \frac{3E_2}{E_1} - \frac{R_1}{3} - \frac{2R_2}{3} \tag{12d}$$

$$u_3 = \frac{\sqrt{3}}{2}\left(\frac{E_1}{6} + 6\frac{E_2}{E_1}\right) \tag{12e}$$

are real numbers, and $i = \sqrt{-1}$. We see that the eigenvalue λ_1 is a real number, $\lambda_{2,3}$ are complex conjugates ($u_2 \pm iu_3$), and λ_4 is 0.

As long as the eigenvalues of the matrix **A** are distinct (Eq. (10)), according to Theorem 6.1, we have

$$\begin{aligned} e^{\mathbf{A}t} &= e^{\lambda_1 t}\frac{\mathbf{A}(\mathbf{A}-\lambda_2\mathbf{I})(\mathbf{A}-\lambda_3\mathbf{I})}{\lambda_1(\lambda_1-\lambda_2)(\lambda_1-\lambda_3)} + e^{\lambda_2 t}\frac{\mathbf{A}(\mathbf{A}-\lambda_1\mathbf{I})(\mathbf{A}-\lambda_3\mathbf{I})}{\lambda_2(\lambda_2-\lambda_1)(\lambda_2-\lambda_3)} + \\ &\quad e^{\lambda_3 t}\frac{\mathbf{A}(\mathbf{A}-\lambda_1\mathbf{I})(\mathbf{A}-\lambda_2\mathbf{I})}{\lambda_3(\lambda_3-\lambda_1)(\lambda_3-\lambda_2)} + \frac{(\mathbf{A}-\lambda_1\mathbf{I})(\mathbf{A}-\lambda_2\mathbf{I})(\mathbf{A}-\lambda_3\mathbf{I})}{-\lambda_1\lambda_2\lambda_3} \end{aligned} \tag{13}$$

$$\equiv e^{\lambda_1 t}\mathbf{L}_1(\mathbf{A}) + e^{\lambda_2 t}\mathbf{L}_2(\mathbf{A}) + e^{\lambda_3 t}\mathbf{L}_3(\mathbf{A}) + \mathbf{L}_4(\mathbf{A}) \tag{14}$$

where **I** is a 4×4 identity matrix, the notation $\equiv$ indicates that (14) serves to define $\mathbf{L}_1(\mathbf{A})$, $\mathbf{L}_2(\mathbf{A})$, $\mathbf{L}_3(\mathbf{A})$, and $\mathbf{L}_4(\mathbf{A})$, the Lagrange

[1] http://www.maplesoft.com.

interpolation coefficients which are called projection operators or projectors in [4,5].

The solution of $e^{\mathbf{A}t}$ can be seen as a sum of three matrices with entries of real numbers: one matrix $e^{\lambda_1 t}\mathbf{L}_1(\mathbf{A})$with decay $e^{\lambda_1 t}$, and one matrix $e^{\lambda_2 t}\mathbf{L}_2(\mathbf{A}) + e^{\lambda_3 t}\mathbf{L}_3(\mathbf{A})$ with decay $e^{u_2 t}$ and oscillation terms $\cos(u_3 t)$, $\sin(u_3 t)$, and the constant matrix $\mathbf{L}_4(\mathbf{A})$. This tells that during a square pulse, the magnetization, for example, M_x, has the following form:

$$M_x(t) = c_1 e^{\lambda_1 t} + (c_2 \sin(u_3 t) + c_3 \cos(u_3 t)) e^{u_2 t} + c_4 \tag{15}$$

where c_j ($j = 1 \cdots 4$) are independent of the time t, but depend on the spin system, the initial state, the strength and phase of the rf field. This form of the solution of the Bloch equations has been displayed in [11]. Furthermore, Eq. (15) tells us that even if $t \gg T_2$, the transverse magnetization may not fall to 0 and the value will be c_4, which has been observed in [44]. The oscillations of Eq. (15) are suppressed or cancelled out if there are three real roots of $p_{\mathbf{A}}(\lambda) = 0$ which are equivalent to the conditions discussed by Torrey [11].

Eq. (13) is the exact algebraic solution of the Bloch equations and will be referred to as Model 0 in this paper. Substituting λ from Eqs. (10)–(12) into Eq. (13) and expanding the multiplication of matrices yeilds an explicit solution which is still inconvenient to work with. Partial substitution, maintaining λ_1, u_2, u_3, E_1, E_2 and E_3 as named subexpressions (unsubstituted variables) results in a manageable expression.

It is easy to verify that Eq. (13) is also the solution of the free evolution when setting b_1 to *0* in the matrix **A** and Eqs. (10)–(12) (see Appendix B). We cannot simply set ω, R_1 and R_2 of the matrix **A** to be zero to get the solution of a hard pulse by Eq. (13) because the eigenvalues are not distinct, but the solution of a hard pulse has been widely known as a rotation matrix. In fact, for these two cases, the solutions can be directly obtained using simpler methods.

When R_1 is equal to R_2, the eigenvalues of the matrix **A** are simple, and the explicit symbolic solution of $e^{\mathbf{A}t}$ by expanding the Lagrange interpolations is completely demonstrated in Appendix C. Setting $R_1 = R_2$ in Eq. (10) gives the first-order approximation of the eigenvalues with respect to the ratio R_1/R_2 evaluated at $R_1/R_2 = 1$, thus the solution of the case of $R_1 = R_2$ also can be seen as a first-order approximation of the general solution of the Bloch equations, which will be discussed in the next section. In the $R_1 = R_2$ case, even if $\gamma\mathbf{B_1}$ is time-varying, the solution of the Bloch equations also can be expressed in a simple way [45].

We can reduce the complexity of the solution by making approximations. Two different methods are displayed in the next section. One method is to use exact solutions corresponding to approximate eigenvalues, another way is to apply the split-operator method to compute the exponential of a matrix.

3. Approximate solutions of the Bloch equations

3.1. Approximate solutions via approximate eigenvalues

The preceding section gives a method to exactly solve the Bloch equations, but it is difficult to manipulate the general solution if intermediate variables are not used. The first- and second-order approximations of eigenvalues can be applied to calculate approximations of the solution of the Bloch equations by substituting λ with Eqs. (17) and (18) into Eq. (13), respectively. These approximations have simpler expressions than the exact solution, but it may be still a challenge to observe interactions between magnetization, spin systems and pulses [11].

Because $R_1 \leqslant R_2$ for all spins, supposing $R_1 = \mu R_2$, $0 < \mu \leqslant 1$, thus $0 \leqslant 1 - \mu < 1$. The second-order Taylor series of λ_1, u_2 and u_3 with respect to μ evaluated at $\mu = 1$ are

$$\lambda_1 \approx -R_2 - \frac{\omega^2 R_2}{b_1^2 + \omega^2}(\mu - 1) + O((\mu - 1)^2) \tag{16a}$$

$$u_2 \approx -R_2 - 1/2\frac{b_1^2 R_2}{b_1^2 + \omega^2}(\mu - 1) + O((\mu - 1)^2) \tag{16b}$$

$$u_3 \approx \sqrt{b_1^2 + \omega^2} + O((\mu - 1)^2) \tag{16c}$$

Eqs. (16a) and (16b) correspond to Eqs. (8) and (9) of [11], and they are used as $-R_{1\rho}$ [46] and $-R_{2\rho}$ [47], respectively. In fact, Eqs. (11a) and (12d) should be exact expressions of $-R_{1\rho}$ and $-R_{2\rho}$.

These give us the first-order approximation of the eigenvalues

$$\boldsymbol{\lambda} \approx \begin{bmatrix} -R_2 \\ -R_2 + i\sqrt{b_1^2 + \omega^2} \\ -R_2 - i\sqrt{b_1^2 + \omega^2} \\ 0 \end{bmatrix} \tag{17}$$

and the second-order approximation of the eigenvalues

$$\boldsymbol{\lambda} \approx \begin{bmatrix} -\frac{b_1^2}{b_1^2+\omega^2}R_2 - \frac{\omega^2}{b_1^2+\omega^2}R_1 \\ -\frac{b_1^2+2\omega^2}{2(b_1^2+\omega^2)}R_2 - \frac{b_1^2}{2(b_1^2+\omega^2)}R_1 + i\sqrt{b_1^2 + \omega^2} \\ -\frac{b_1^2+2\omega^2}{2(b_1^2+\omega^2)}R_2 - \frac{b_1^2}{2(b_1^2+\omega^2)}R_1 - i\sqrt{b_1^2 + \omega^2} \\ 0 \end{bmatrix} \tag{18}$$

with respect to the ratio R_1/R_2 evaluated at $R_1/R_2 = 1$. We see that the second-order approximation of λ_1 is the same as $-R_{1\rho}$ given by Eq. (1) of [46].

Commonly, R_1 is much smaller than R_2 so we simply set $R_1 = 0$ in the eigenvalues, and set $R_2 = \delta b_1$, then the Taylor series of λ_1, u_2 and u_3 with respect to δ evaluated at $\delta = 0$ is

$$\lambda_1 \approx -\frac{b_1^3}{b_1^2 + \omega^2}\delta + O(\delta^3) \tag{19a}$$

$$u_2 \approx -1/2\frac{b_1\left(b_1^2 + 2\omega^2\right)}{b_1^2 + \omega^2}\delta + O(\delta^3) \tag{19b}$$

$$u_3 \approx \sqrt{b_1^2 + \omega^2} + O(\delta^2) \tag{19c}$$

and the eigenvalues can be approximated as

$$\boldsymbol{\lambda} \approx \begin{bmatrix} -\frac{b_1^2 R_2}{b_1^2+\omega^2} \\ -1/2\frac{\left(b_1^2+2\omega^2\right)R_2}{b_1^2+\omega^2} + i\sqrt{b_1^2 + \omega^2} \\ -1/2\frac{\left(b_1^2+2\omega^2\right)R_2}{b_1^2+\omega^2} - i\sqrt{b_1^2 + \omega^2} \\ 0 \end{bmatrix} \tag{20}$$

which can be obtained from Eq. (18) by setting $R_1 = 0$.

If we set $R_1 = 0$ and $R_2 = \beta\omega$, we get the Taylor series of λ_1, u_2 and u_3 with respect to β evaluated at $\beta = 0$ as

$$\lambda_1 \approx -\frac{\omega b_1^2}{b_1^2 + \omega^2}\beta + O(\beta^3) \tag{21a}$$

$$u_2 \approx -1/2\frac{\omega\left(b_1^2 + 2\omega^2\right)}{b_1^2 + \omega^2}\beta + O(\beta^3) \tag{21b}$$

$$u_3 \approx \sqrt{b_1^2 + \omega^2} + O(\beta^2) \tag{21c}$$

and the approximate eigenvalues are the same as Eq. (20).

Eq. (15) demonstrates that the magnetization within a square pulse is a combined decay rather than a single decay, but the first-order approximations of the eigenvalues (Eq. (17)) display that the magnetization during a square pulse mostly is affected

by the effective rf field $\sqrt{b_1^2+\omega^2}$ while the decay rate is approximate to R_2. The second-order approximation of the eigenvalues (Eq. (18)) clearly shows how the decay rates during a square pulse are influenced by the rf field and the offset.

3.2. Approximate solutions via split-operators

In this subsection, we compute $e^{\mathbf{A}t}$ using the split-operator method and explore its implications to understanding soft pulses. When $\mathbf{X}$ and $\mathbf{Y}$ do not commute (i.e. $[\mathbf{X},\mathbf{Y}] \equiv \mathbf{X}\cdot\mathbf{Y}-\mathbf{Y}\cdot\mathbf{X} \neq \mathbf{0}$), $e^{(\mathbf{X}+\mathbf{Y})t} \neq e^{\mathbf{X}t}e^{\mathbf{Y}t}$. But understanding the quality of this approximation and the nature of the error is still instructive. This approach has been applied in quantum mechanics [48,49] and in discussions of excitation pulses [23].

In the following, we compute the approximations of $e^{\mathbf{A}t}$ by applying the second-order split-operator approximation of $e^{(\mathbf{X}+\mathbf{Y})t}$ [48] which is

$$e^{(\mathbf{X}+\mathbf{Y})t} \approx e^{(t/2)\mathbf{X}}e^{(t)\mathbf{Y}}e^{(t/2)\mathbf{X}} \tag{22}$$

Since it is a sum of three matrices $\boldsymbol{\Omega}$, $\gamma\mathbf{B_1}$ and $\mathbf{R}$, the matrix $\mathbf{A}$ can be split into three combinations as a sum $\mathbf{X}+\mathbf{Y}$,

$$\mathbf{A} = (\boldsymbol{\Omega}+\mathbf{R})+\gamma\mathbf{B_1} \tag{23a}$$
$$= (\boldsymbol{\Omega}+\gamma\mathbf{B_1})+\mathbf{R} \tag{23b}$$
$$= \boldsymbol{\Omega}+(\gamma\mathbf{B_1}+\mathbf{R}) \tag{23c}$$

Eq. (22) shows that we have two approximations if we change the order of $\mathbf{X}$ and $\mathbf{Y}$. So there are six approximate solutions of the Bloch equations by the second-order split-operator method,

$$\mathbf{A} = (\boldsymbol{\Omega}+\mathbf{R})+\gamma\mathbf{B_1} \equiv \mathbf{X}_1+\mathbf{Y}_1 \quad \text{(Model 1)} \tag{24a}$$
$$\mathbf{A} = \gamma\mathbf{B_1}+(\boldsymbol{\Omega}+\mathbf{R}) \equiv \mathbf{X}_2+\mathbf{Y}_2 \quad \text{(Model 2)} \tag{24b}$$
$$\mathbf{A} = \mathbf{R}+(\boldsymbol{\Omega}+\gamma\mathbf{B_1}) \equiv \mathbf{X}_3+\mathbf{Y}_3 \quad \text{(Model 3)} \tag{24c}$$
$$\mathbf{A} = (\boldsymbol{\Omega}+\gamma\mathbf{B_1})+\mathbf{R} \equiv \mathbf{X}_4+\mathbf{Y}_4 \quad \text{(Model 4)} \tag{24d}$$
$$\mathbf{A} = \boldsymbol{\Omega}+(\gamma\mathbf{B_1}+\mathbf{R}) \equiv \mathbf{X}_5+\mathbf{Y}_5 \quad \text{(Model 5)} \tag{24e}$$
$$\mathbf{A} = (\gamma\mathbf{B_1}+\mathbf{R})+\boldsymbol{\Omega} \equiv \mathbf{X}_6+\mathbf{Y}_6 \quad \text{(Model 6)} \tag{24f}$$

Note that $\mathbf{X}_1=\mathbf{Y}_2$, $\mathbf{Y}_1=\mathbf{X}_2$, $\mathbf{X}_3=\mathbf{Y}_4$, $\mathbf{Y}_3=\mathbf{X}_4$, $\mathbf{X}_5=\mathbf{Y}_6$, and $\mathbf{Y}_5=\mathbf{X}_6$, but substituting them into Eq. (22) will give different approximations of $e^{\mathbf{A}t}$. All of the exponentials of these split matrices $t\mathbf{X}_j$, $t\mathbf{Y}_j$ (j from 1 to 6) can be easily calculated by classical methods, then Eq. (22) is applied to compute $e^{\mathbf{A}t}$. Error analysis shows that Model 5 is close to Model 1, and Model 6 is close to Model 2, so in the following, we will not analyse Models 5 and 6.

Calculating these approximations of $e^{\mathbf{A}t}$ can be seen as dealing with a soft pulse as different pseudo-pulse sequences. Without loss of generality, a soft π pulse is used in the Hahn echo to illustrate these split-operators which are shown in Fig. 4.

If the spin is on-resonance, i.e. $\omega = 0$, Model 1 will be the same as Model 3, and Model 2 will be the same as Model 4. Suzuki has shown that the error of the approximation $e^{(t/2)\mathbf{X}}e^{(t)\mathbf{Y}}e^{(t/2)\mathbf{X}}$ of $e^{(\mathbf{X}+\mathbf{Y})t}$ is bounded and the upper bound can be computed by Theorem 6.2 [49]. Comparing expressions and upper bounds of errors (not shown), when all of offsets and relaxation rates are smaller than the amplitude of the pulse then, in general, the error bounds improve in the order: Model 1, Model 2, Model 3, Model 4, but expression complexity goes up in the same order. Figs. 1 and 2 demonstrate relative errors of approximations of a soft π pulse against the ratio of the offset over the amplitude of the pulse for given numerical relaxation parameters. The figures show that errors of Model 3 and Model 4 (where rotation is around the effective field) are much smaller than errors of Model 1 and Model 2 (in which the rotation axis is in the xy plane). The errors of Model 1 and Model 2 increase rapidly with the ratio of $\|\omega/\gamma B_1\|$ being almost linear on the interval $[-1,1]$, while the errors of Model 3 and Model 4 are smooth and bounded in this interval. The difference of errors of Model 3 and Model 4 is very small when the offset is smaller than the amplitude of the pulse. Splitting the matrix $\mathbf{A}$ into the effective rotation field and relaxation terms provides a good approximation to a soft pulse when the relaxation ratios are much smaller than the amplitude of the pulse.

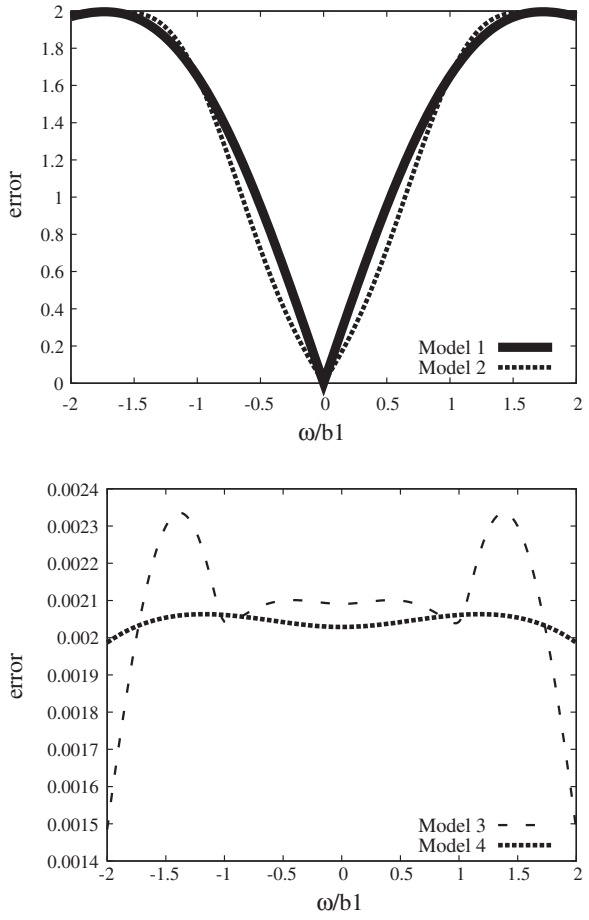

Fig. 1. Comparing relative errors of different approximations. The relative errors are calculated as $\|e^{(\mathbf{X}+\mathbf{Y})t}-e^{(t/2)\mathbf{X}}e^{(t)\mathbf{Y}}e^{(t/2)\mathbf{X}}\|_2/\|e^{(\mathbf{X}+\mathbf{Y})t}\|_2$, the x axis is the ratio of offset to pulse amplitude (when both are measured in Hz). The numerical computation uses the dimensionless parameters, $b1 = 2000$ Hz, $t_p = 1/(2b_1)$, $\phi = 0$, $R_2/b_1 = 0.01$, $R_1/R_2 = 0.2$. The figures show that if the absolute value of the offset is smaller than the amplitude of the pulse, the relative errors of Model 3 and Model 4 are much smaller than errors of Model 1 and Model 2. The large error of Models 1 and 2 are mainly due to the fact that z magnetization are poorly described.

4. Computation of experiments of the Hahn echo

In this section, we will apply the exact and approximate solutions of the Bloch equations to explore effects of a soft echo pulse on the transverse magnetization. Fig. 3 shows the pulse sequence of the Hahn echo experiments [50]. We will concentrate on investigating soft echo pulses, so in the simulations and experiments of Hahn echo experiments, the excitation $\pi/2$ pulse is approximated by a hard pulse along with the y axis, this means the magnetization vector after the excitation pulse is $\mathbf{M_0} = [1,0,0,1]^T$. Therefore, the

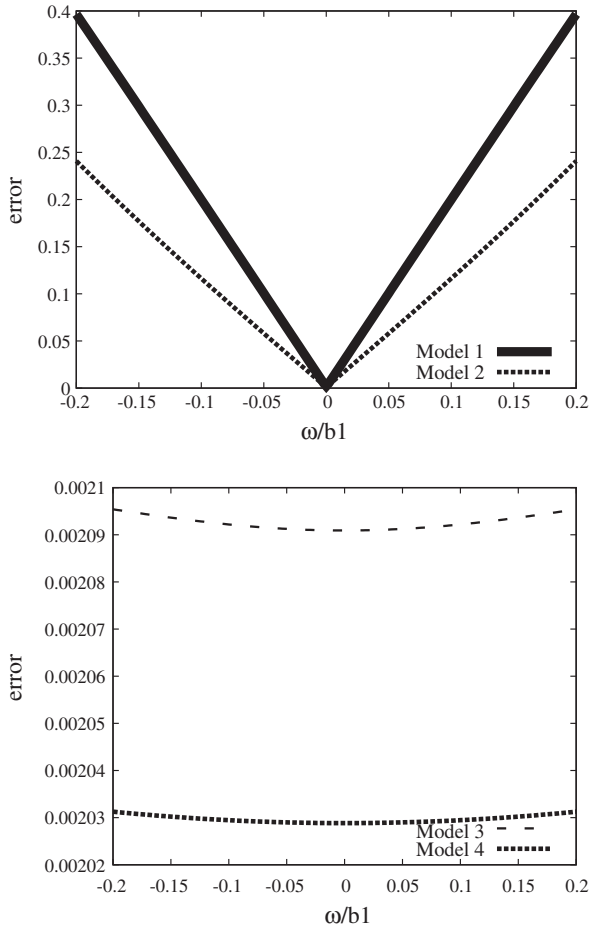

Fig. 2. Comparing relative errors of different approximations. Labels are the same as in Fig. 1. The range of pulse amplitude/offset (on the x axis) is restricted to −0.2 to 0.2. This figure demonstrates that even for offsets close to on-resonance, the errors of Model 1 and Model 2 are much bigger than errors of Model 3 and Model 4.

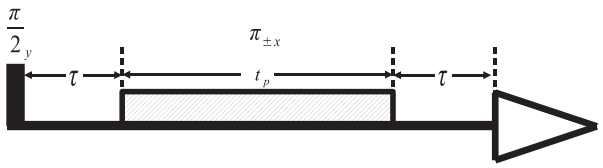

Fig. 3. The pulse sequence of the Hahn echo experiments. Without loss of generality, the excitation $\pi/2$ pulse is set as a hard pulse along with the y axis. The delay time between the excitation pulse and the echo pulse is τ. The length of the soft π pulse is t_p and the phase cycling scheme of $\pm x$ is applied in our experiments and simulations.

magnetization or the intensity at the beginning of the acquistion is a function of seven variables: τ, t_p, b_1, ω, ϕ, R_1 and R_2. The complicated behaviour of the function can be seen from Figs. 6 and 7.

The magnetization at the end of the evolution is computed by

$$\mathbf{M_t} = \mathbf{Exp}(\mathbf{A_{FID}}) \cdot \mathbf{Exp}(\mathbf{A}_\pi) \cdot \mathbf{Exp}(\mathbf{A_{FID}}) \cdot \mathbf{M_0} \tag{25}$$

where $\mathbf{Exp}(\mathbf{A_{FID}})$ (Eq. (B.2)) represents the effective matrix of the free evolution, $\mathbf{Exp}(\mathbf{A}_\pi)$ the effective matrix of a π pulse, which can be the exact solution or approximate solutions of the soft π pulse.

If phase cycling is applied in the experiment, the effective matrix $\mathbf{Exp}(\mathbf{A}_\pi)$ will be the average of the effective matrices for all phases. Eqs. (C.5) and (D.1) show that phase cycling of $\pm x$ can be used to make the constant term c_4 of Eq. (15) zero and c_1, c_2 and c_3 independent of the z magnetization which means that the effect of the longitudinal magnetization on the transverse magnetization within a square pulse is eliminated, see also [51,52], this may be helpful to improve the sensitivity of the spectra [53] and the accuracy of the measurements of R_1 and R_2 by 5–15% over the case where the constant term is not included in the data analysis [51], and complete the coherence selection [54].

In Appendix D, $\mathbf{M_t}$ is calculated with phase cycling or different phases with exact and approximate solutions of the Bloch equations. In order to simplify the notations, Model 0 will also be used to represent the exact solution of the Hahn echo with the exact symbolic solution of the Bloch equations of a square pulse, Models 1–4 represent approximate solutions of the Hahn echo with approximate solutions of the Bloch equations of a square pulse which are computed by Eq. (22) with four different operator splitings (Eqs. (24a)–(24d)) which can be seen as four different pseudo-pulse sequences (Fig. 4), respectively.

Generally, the explicit expression of the magnetization $\mathbf{M_t}$ with respect to the offset, true R_1 and R_2, delay time, the pulse length, the phase of the pulse, and the amplitude of the pulse can be obtained by substituting the explicit expression of the effective matrix of a soft π pulse (Eq. (14)) into Eq. (25). As we said before, this explicit expression of $\mathbf{M_t}$ will be huge even with the phase cycling. The implicit symbolic expressions of the transverse magnetization of the Hahn echo of a phase cycle of π pulses are given by Eq. (D.3).

Model 1 approximation can be seen as an echo experiment of delay $(\tau + t_p/2)$ of using a hard π pulse, thus, the transverse magnetization given by this approximation at the beginning of the acquisition will be along with the x axis and its value will be partial of $e^{-R_2(2\tau+t_p)}$. Mathematically, we could say this approximation is the first-order approximation of the Hahn echo of a soft echo pulse with respect to the offset at the on-resonance.

In Model 2 approximation, a soft π pulse is approximated by two hard $\pi/2$ pulses and a free evolution between the two $\pi/2$

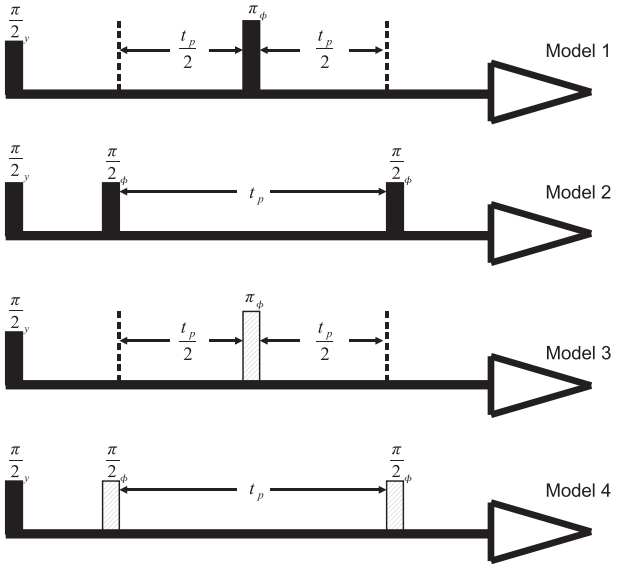

Fig. 4. The approximations of the Hahn echo. The black rectangles represent hard pulses, the hatching rectangles represent effective rotations. In Model 1, the soft echo π pulse is approximated by a hard π pulse with two delays of $t_p/2$; in Model 2, the soft echo π pulse is approximated by two $\pi/2$ hard pulses with a delay t_p; in Model 3, the soft echo π pulse is approximated by an effective rotation of $t_p\sqrt{b_1^2+\omega^2}$ with two on-resonance delays of $t_p/2$; in Model 4, the soft echo π pulse is approximated by two effective rotations of $\frac{t_p}{2}\sqrt{b_1^2+\omega^2}$ with one on-resonance delay of t_p.

pulses. If spins are not on-resonance, this approximation tells us that spins will not refocus on the x axis. The magnetization before the acquisition is easy to compute because the effect of a hard pulse is equivalent to a rotation matrix. Appendix D.2 displays expressions of the transverse magnetizations of approximations of Model 2 with different phases of the echo pulses. As we see from Figs. 1 and 2, Models 1 and 2 approximate the Hahn echo well when the offset is negligible compared to the amplitude of the echo pulse.

Model 3 approximation is similar to Model 1 approximation except that it uses the effective rotation field. This model shows the effect of offsets during a π pulse. Eqs. (D.11), (D.13) and (D.14) give the explicit solutions of effective rotations during a finite pulse of different phases. The calculation shows that the expressions of the transverse magnetization given by Model 3 are the explicit exact solution of the Hahn echo of the case $R_1 = R_2$ when the phase cycling of $\pm x$ is applied.

Based on the computation of Model 3, the approximation of Model 4 is easily computed (see Appendix D.4). Basically, the error of this approximation is a little smaller than the one of Model 3 when the offset is smaller than the amplitude of the echo pulse (see Figs. 1 and 2), but the expressions of the transverse magnetization are more complicated than the solutions given by Model 3.

5. Measuring R_2 by the Hahn echo

Measuring transverse relaxation R_2 with NMR and MRI is required to estimate the motion of molecules and other dynamical investigations [18], but making accurate R_2 estimates is a challenge due to the pulse imperfections, offset, delay, B_0 and B_1 inhomogeneity, etc. The two main methods are the Hahn echo method [50], and the CPMG pulse sequence [55]. Ideally, they have identical echo envelopes for viscous samples with negligible diffusion [56]. Although the CPMG method self-corrects for pulse inaccuracy [55], it is not a trivial matter to eliminate the systematic cumulative errors in the multiple pulse experiments due to other pulse imperfections [51,52,57–59], even using hard echo pulses, the measured R_2 may be unreliable if $\|\omega\| > 0.1\gamma B_1$ [51]. Theoretically, in CPMG experiments, the sample needs to start from the equilibrium only once, but in practice, the sample also needs to return to its equilibrium condition each time for every measurement. Thus, CPMG experiments may not save experiment time. For these reasons and to simplify the calculations, we restrict our method on the Hahn echo to measure the transverse relaxation rate in this paper.

Most previous research which analyzed the error of measured R_2 focused on the offset effects [51,58,59]. But the use of cryoprobes, further restricts the amplitude of π pulses, forcing them to be longer-potentially as long as the delay time between the excitation pulse and the echo pulse [18]. In this new situation, relaxation must be considered in addition to the effect of offset. Phase cycling techniques have been applied to correct measurements of R_2 for long π pulses [18,60]. Because of the difficulty of getting the symbolic solution of Bloch equations, these previous studies used numerical simulations, rotation matrices or $R_{1\rho}$ to analyze or correct errors of R_2.

Generally, the measurement of R_2 is obtained by solving the following least-square optimization problem,

$$\min \|M_{\text{meas}}(t) - M_{\text{sim}}(t)\|^2 \tag{26}$$

where $M_{\text{meas}}(t)$ is the measured amplitude of the transverse magnetization at the time point t which is acquired from the experiment, $M_{\text{sim}}(t)$ is the calculated amplitude of the transverse magnetization at the time point t using one of the models. The amplitude of the transverse magnetization is defined as $\sqrt{M_x^2 + M_y^2}$. We fit the *magnitude* of the transverse magnetization rather than the x and y components separately in order to simplify the optimization problem by eliminating both the numerical and experimental problems associated with phase. The objective function in the added phase dimensions would be highly non-convex, with multiple local minima, introducing a new failure mode for the optimization software. While using the individual transverse components has, in principle, the effect of taking an extra average, in practice, various phase errors associated with timing problems need to be corrected, so the maximum benefit would be less.

In the classical method to fit R_2, the fitting function which could be seen as Model 1 is

$$M(t) = M(0)e^{-R_2 t} \tag{27}$$

Because the fitting function (Eq. (27)) does not include effects of other parameters such as offsets, pulse amplitude, pulse phase, and R_1, systematic errors of measurements of R_2 which are associated with these factors cannot be eliminated. Suppressing these errors of the measurement of R_2 is very difficult [18,51,52,57–60]. Figs. 1 and 2 show expected errors from Model 1 in excess of 20% when $\|\omega/\gamma B_1\| > 0.1$ making R_2 estimates meaningless [51].

In this section, we replace the function to fit ($e^{-R_2 t}$) with the exact symbolic solution of the Bloch equations.

If the Hahn echo experiments with n different delay times are completed, the fitting optimization problem to measure R_2 is

$$\min \sum_{j=1}^{n} \left\| M_{\text{meas}}(j) - I_0 \sqrt{M_{x,j}^2 + M_{y,j}^2} \right\|^2 \tag{28}$$

where $M_{\text{meas}}(j)$ is the measured amplitude of the transverse magnetization of the delay time τ_j. $M_{x,j}$ and $M_{y,j}$ will be calculated by Eq. (25) in which $\mathbf{Exp}(\mathbf{A}_\pi)$ is generated by the exact solution of the Bloch equations.

The fitting optimization problem is usually unconstrained if all of intermediate variables are substituted. For example, an unconstrained optimization problem for the Hahn echo experiment with echo pulses of a phase cycling of $\pm x$ can be configured by substituting $M_{x,j}$, $M_{y,j}$ and other intermediate variables with Eqs. (11), (12), (D.2) and (D.3) in Eq. (28). In this unconstrained optimization problem, only I_0 and R_2 are variables, ω, b_1, t_p, R_1, τ_j, $M_{\text{meas}}(j)$ are parameters. To solve this unconstrained problem, a lot of memory and more time may be required to store and calculate the huge objective function.

On the other hand, equivalent constrained optimization problems can be developed to dramatically reduce the size of the objective function and eliminate the computation of redundant terms so as to improve the efficiency of solving the problem. For example, if replacing $M_{x,j}$ and $M_{y,j}$ in the optimization problem (28) with Eq. (D.3), keeping other intermediate variables, making Eqs. (11), (12), and (D.2) as equality constraints, an equivalent constrained optimization problem to measure R_2 of applying the Hahn echo with a phase cycling $\pm x$ can be constructed.

The fitting problem is extremely nonlinear due to the oscillation. Despite this, we note that the first- and second-order approximations of the eigenvalues show that the oscillation is significantly effected by the offset but not by the relaxation rates, which suggests that the fitting problem may nevertheless be solvable. This also can be seen in the fitting function given by Model 3 which shows that R_2 appears alone in the exponential function when a phase cycling scheme is employed (see Eq. (D.12)). These observations are validated by plotting the contour of the objective function with respect to I_0 and R_2 (Fig. 5).

Errors in measured R_2 caused by magnet field inhomogeneities can be small to moderate and the upper bounds of these errors may be determined experimentally [61], but because ω and b_1 are independent parameters in our models, B_0 and B_1 inhomogene-

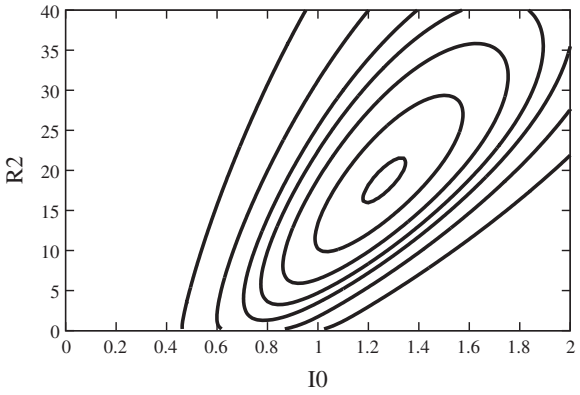

Fig. 5. Contour of the objective function with respect to I_0 and R_2. The objective function (without B_0 inhomogeneity) corresponds to fit the experiment of the offset −503 Hz in Fig. 6. This figure shows that the fitting problem has a solution within $R_2 \in [0,40]$ and $I_0 \in [0,2]$. When solving the fitting problem, R_2 and I_0 are not given the upper bound.

ities could be taken into account if the distributions of the inhomogeneities are known by experiment [62]. The calculated transverse magnetization will be the average transverse magnetization computed for different B_0 and B_1 fields.

In the data analysis, optimization models were written in A Modeling Language for Mathematical Programming (AMPL[2]) [63], and solved using Interior Point OPTimizer (IPOPT[3]) [64]. All solver and parameter options were kept constant, including the initial values.

5.1. Experiments

A series of experiments were performed on a Bruker AVANCE I 500 MHz spectrometer with a Shigemi tube at different temperatures, the sample was cyclohexane and the solvent was $CDCl_3$, the temperatures were adjusted to 280 K or 279 K, in order to obtain an appropriate R_2. The amplitude of the echo pulse was equivalent to 500 Hz. The duration of the echo pulse was 0.001 s. The measured R_1 was 0.22 s^{-1} at 280 K. Two sets of delay times were used at two different temperatures, the first set at 280 K had 54 delays of $0.0005 \times j$ ($j = 1 \cdots 49$) and $\{0.03, 0.04, 0.05, 0.06, 0.5\}$ seconds, the second set at 279 K includes 234 delays of $0.0001 \times j$ ($j = 1 \cdots 100$), $0.01 + 0.001 \times j$ ($j = 1 \cdots 90$), $0.1000 + 0.0001 \times j$ ($j = 1 \cdots 40$) and $\{0.2, 0.3, 0.4, 0.5\}$ seconds. The duration of the excitation pulse was 8.25 μs and the strength of the excitation pulse was equivalent to 30,300 Hz. A CPMG experiment with high-power pulses and the signal on-resonance gave an R_2 which was the same as the Hahn echo with the signal on-resonance. The phase cycling of $\pm x$ of echo pulses was applied in the Hahn echo pulse sequence. The measured intensities were obtained by the TOPSPIN software.

True R_2 values are independent of offset, but both of Figs. 6 and 7 show that R_2 estimates based on measurements vary for large offsets, and more sampling points do not help to improve the fitting results, so the problem is not related to measurement uncertainty related to the Nyquist sampling criterion for oscillating signals. After analyzing and numerically simulating the experiments, we find that the dense sampling does not help to improve the measurements of R_2. In fact, only B_0 inhomogeneity can explain the errors in the R_2 estimates from our experiments.

In order to analyze effects of the inhomogeneity, the magnetic field inhomogeneity was estimated by the experiment *popt* which is the parameter optimization on Bruker spectrometers. The measured intensity at 810° is approximate to 92% of the intensity at 90° with the initial pulse length 2.5 μs and the increasing step 2.5 μs under the equivalent power 30,300 Hz. Normally, B_0 and

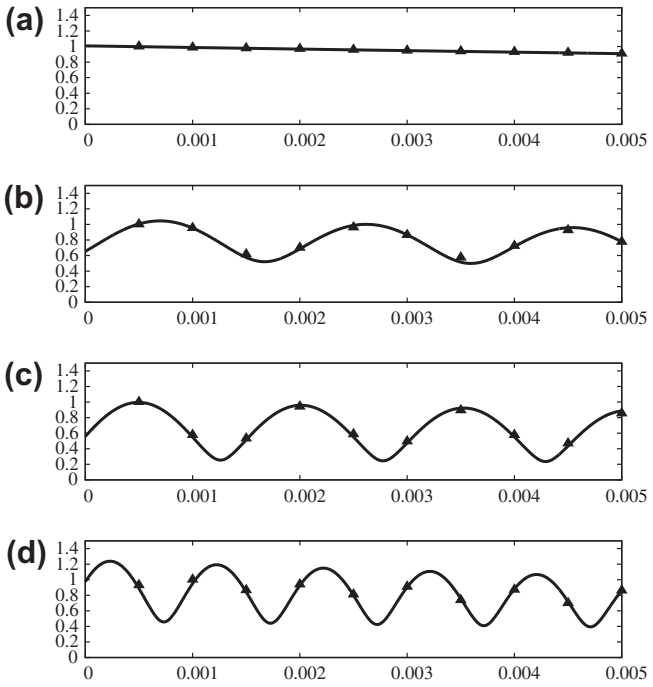

Fig. 6. Fitted curves and measured intensities. The x axis is the delay time τ in seconds, the y axis is the intensity, normalized so that the maximum measured intensity is 1. The triangles are measured intensities, the curves are the result of fitting Model 0 (without B_0 inhomogeneity). The experiments were performed at 280 K. The offsets are 0.0, −260, −330, and −503 Hz, the measured R_2 are 10.46,11.19,12.64, and *18.68* s^{-1}, respectively. In all cases, $R_1 = 0.22$ s^{-1}.

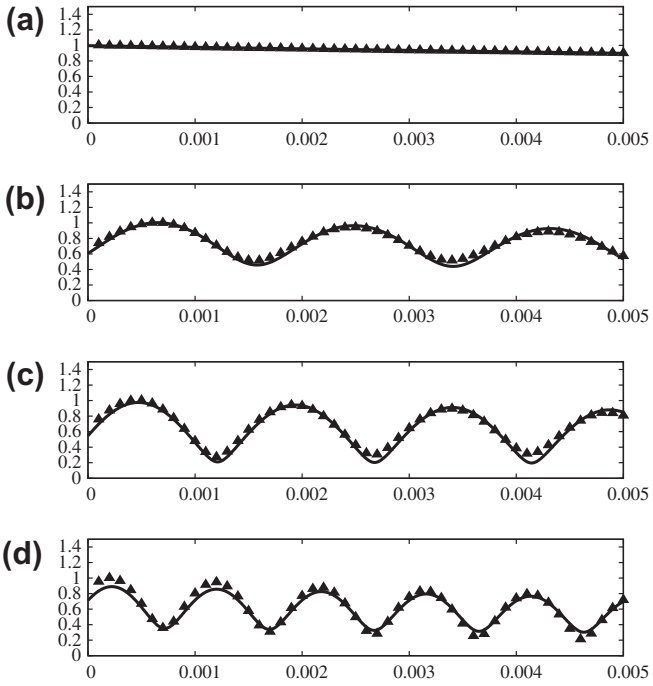

Fig. 7. Fitted curves and measured intensities, using denser sampling. Labelled as in Fig. 6. The offsets are 0.0, −273, −341, and −511 Hz, the measured R_2 are 10.35, 10.73, 11.60, and 19.15 s^{-1}, respectively. In all cases, $R_1 = 0.22$ s^{-1} and temperature 279 K.

[2] http://www.ampl.com/; student version 20091101.
[3] http://projects.coin-or.org/Ipopt; version: 3.8.1.

B_1 inhomogeneity are correlated, in order to simplify the discussion, we separately simulate B_0 and B_1 inhomogeneity in the following.

To simulate the B_0 inhomogeneity, 15 relative offsets $\{-4 + 8j/14\}$ Hz, j from 0 to 14, with respect to $O1$ which is a parameter on Bruker spectrometers to represent the irradiation frequency offset for the frequency channel $f1$ in Hz were chosen, weighted by the Gaussian distribution $e^{-(x-\mu)^2/(2\delta^2)}/\sqrt{2\pi\delta^2}$ with $\mu = 0$ and $\delta = 2$. Another way of characterizing this assumption is that the full width of the relative offset with respect to $O1$ at the half height of the Gaussian distribution is 4.7 Hz. The calculated magnetization is the sum of the products of the weight and the magnetization corresponding to the relative offset. With these assumptions, the predicted intensity at 810° is 95% of the intensity at 90°. Comparing the simulation with inhomogeneity to those without inhomogeneity, we have observed that the value of the objective function, which measures the fit between the model and the measurements, would be reduced by over 30% but the accuracy of the R_2 estimate may be improved by 10%. If the B_0 inhomogeneity is described more close to the real experiment, the fitting result may be improved. Fig. 8 displays the results with and without B_0 inhomogeneity in the models.

Similarly, we simulate the B_1 inhomogeneity using a combination of seven rf amplitudes weighted by the Gaussian distribution in place of each discrete rf pulse. The calculated magnetization is the sum of the products of the weight and the magnetization corresponding to the rf amplitude. The rf scalers are $\{0.95, 0.97, 0.99, 1.0, 1.01, 1.03, 1.05\}$, the normalized weights which are calculated by the Gaussian distribution with $\mu = 1$ and $\delta = 0.023$ are $\{0.024, 0.110, 0.236, 0.260, 0.236, 0.110, 0.024\}$. With this approximation of the B_1 inhomogeneity, the calculated intensities match the intensities of the real experiments well. But the effect on the estimated R_2 values is not significant, both using real and simulated data.

5.2. Effects of other parameters to the measurements of R_2

Since ω, b_1 and R_1 are parameters in the models, their mis-calibration could also skew our estimates for R_2. It is possible, in principle, to estimate these effects by computing the first-order derivates of the intensity with respect to these parameters, but as previously discussed, the expressions are large, and this approach has been proved intractable. In this subsection, we simulate how variations of these parameters effect R_2 estimates. The results from simulated experiments, even with parameter variations, agree with the results from the previous subsection.

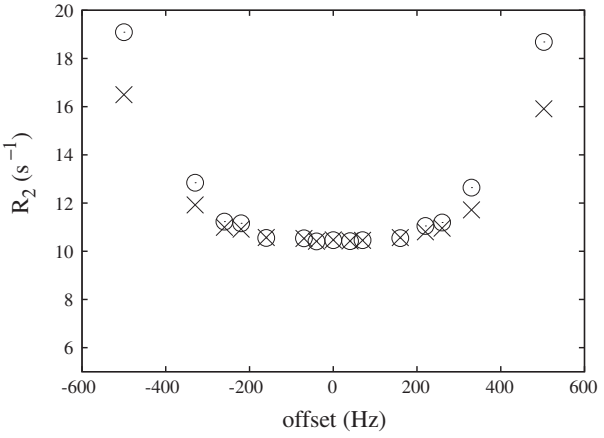

Fig. 8. Estimated R_2 as a function of offset, using the first set of delays at 280 K. Circles are obtained from the model without B_0 inhomogeneity, the cross symbols are obtained from the model including B_0 inhomogeneity. The model with the B_0 inhomogeneity can reduce errors by 10%, giving a reasonable estimate of R_2 within the offsets $\pm 0.7\gamma B_1$. Without B_0 inhomogeneity, but using the exact solution of the Hahn echo, the estimates are still good within $\|\omega\| \leqslant 0.5\gamma B_1$, contradicting the conclusion that R_2s obtained from CPMG may be meaningless when $\|\omega\| > 0.1\gamma B_1$ [51].

The parameters for the simulated experiments are the same as the real experiments with $R_2 = 10.5\ s^{-1}$. From an initial magnetization of $[1,0,0,1]^T$, the intensity was computed using 20-digit precision in Maple, and estimates calculated as above.

In real experiments, the offset may not be exact as we expect due to the unstable B_0 field. The simulation shows that even -2 Hz error of the offset may result in $\sim$10% error of measurements of R_2. This simulation tells us that the stable B_0 field is important for accurately measuring R_2 and the inhomogeneity of the B_0 field has a significant impact on the measurements of R_2.

In experiments, the amplitude of pulses may be mis-calibrated, but the simulation presents that the 2% error of the amplitude of the echo pulse only cause $\sim$1% maximum errors in R_2 when using the phase cycling scheme to acquire the data. These experiments are less sensitive to B_1 inhomogeneity.

The fitting models require an a prior estimate of R_1 to estimate R_2, but the simulations show that the errors in R_2 caused by errors in R_1 are very small, and can be ignored. There are two explanations for this phenomena, one is that the phase cycling eliminates the effect of the z magnetization to the transverse magnetization, another is that we assume the amplitude of the pulse is much bigger than the relaxation rates.

6. Conclusion

In this paper, the general symbolic solution of the Bloch equations is given by the Lagrange form and the explicit solution in the case $R_1 = R_2$ is displayed. Two methods of approximating the solution of the Bloch equations are explained, and error analysis indicates that the methods with the effective rf field (Model 3 and Model 4) are good approximations which have simple expressions. The phase cycling $\{\phi, \phi + \pi\}$ of rectangular pulses will eliminate the effect of the z magnetization on the transverse magnetization during the pulses, this will minimize the errors in measured R_1 and R_2. And this phase cycling scheme also can be extended to the CPMG experiments to minimize the cumulative errors of measurements of R_2 due to pulse imperfections.

We have applied the solutions of the Bloch equations to compute the Hahn echo experiments. With these calculations, models which can exactly describe the experiments have been developed to measure R_2 using more sophisticated mathematical models. Validation against both numerical simulation and actual experiment show that accurate R_2 estimates for $\|\omega\| \leqslant 0.5\gamma B_1$ can be obtained by using maximum likelihood estimates based on an exact algebraic solution of the Bloch equations. If the magnet field B_0 inhomogeneity is added to the models, it is possible to improve the accuracy of the estimates by 10%. More accurate descriptions of the B_0 inhomogeneity may result in further improvements. We also find that the estimates are insensitive to errors in the a priori R_1 values and B_1 inhomogeneity. These models also eliminate the delay dependence discussed in [51,52], allowing delay times shorter than the pulse duration.

In the future, the exact solution of the Bloch equations can be similarly applied to describe arbitrary spin-$\frac{1}{2}$ experiments. For example, it is easy to extend the models of Hahn echo experiments to CPMG experiments recursively. From the point of view of numerical efficiency, it is better to solve constrained problems including subexpressions describing physically meaningful quantities as auxiliary variables, than to eliminate these variables and solve unconstrained problems with fewer variables. We will apply the solution of the Bloch equations and the more general

expansion formula (see Eq. (A.3)) of the projection operator formalism [4] to investigate the CPMG experiments and resulting R_2 estimates, we also will apply the Lagrange form to deal with larger systems with the Liouville space method.

Acknowledgment

Alex D. Bain and Christopher Anand would like to thank the Natural Science and Engineering Research Council of Canada (NSERC) for financial support.

Appendix A. Theorems

The following theorem which was proved in [37] is applied to calculate the explicit solution of $e^{\mathbf{A}t}$.

Theorem Appendix 6.1. *If A is an $n \times n$ matrix with n distinct eigenvalues $\lambda_1, \lambda_2, \ldots, \lambda_n$, then we have*

$$e^{tA} = \sum_{k=1}^{n} e^{t\lambda_k} L_k(A) \tag{A.1}$$

where the $L_k(A)$ are Lagrange interpolation coefficients given by

$$L_k(A) = \prod_{j=1, j\neq k}^{n} \frac{A - \lambda_j I}{\lambda_k - \lambda_j} \tag{A.2}$$

for $k = 1, 2, \ldots, n$.

Löwdin has illustrated a more general expansion formula

$$f(A) = \sum_k f(\lambda_k) L_k(A) \tag{A.3}$$

for any polynomial function f of A and discussed properties of projectors $L_k(A)$ [4]. This general formula can be applied to calculate exact solutions of CPMG experiments.

The following inequality which was proved in [49] gives the boundary for the approximation of $e^{\mathbf{A}t}$ when applying the second-order split method,

Theorem Appendix 6.2. *For any operators* $\mathbf{X}$ *and* $\mathbf{Y}$ *in a Banach algebra,*

$$\left\| e^{\lambda(\mathbf{X}+\mathbf{Y})} - e^{(\lambda/2)\mathbf{X}} e^{(\lambda)\mathbf{Y}} e^{(\lambda/2)\mathbf{X}} \right\| \leqslant \Delta_2(\lambda\mathbf{X}, \lambda\mathbf{Y}), \tag{A.4}$$

where $\Delta_2(\lambda\mathbf{X}, \lambda\mathbf{Y})$ is defined as,

$$\Delta_2(\lambda\mathbf{X}, \lambda\mathbf{Y}) = \hat{\Delta}_2(\lambda\mathbf{X}, \lambda\mathbf{Y}) exp(\|\lambda\mathbf{X}\| + \|\lambda\mathbf{Y}\|) \tag{A.5}$$

$$\hat{\Delta}_2(\lambda\mathbf{X}, \lambda\mathbf{Y}) = \frac{1}{12}\left\{ \|[[\lambda\mathbf{X}, \lambda\mathbf{Y}], \lambda\mathbf{Y}]\| + \frac{1}{2}\|[[\lambda\mathbf{X}, \lambda\mathbf{Y}], \lambda\mathbf{X}]\| \right\} \tag{A.6}$$

Appendix B. Solution of the free evolution

In the Bloch equations, when $b_1 = 0$ which represents the free evolution decay, the eigenvalues of the matrix $\mathbf{A}$ have simple expressions,

$$\boldsymbol{\lambda}(\mathbf{A}(b_1 = 0)) = \begin{bmatrix} -R_1 \\ -R_2 + i\omega \\ -R_2 - i\omega \\ 0 \end{bmatrix} \tag{B.1}$$

where $\boldsymbol{\lambda}(\mathbf{A}(b_1 = 0))$ stands for the eigenvalues of the matrix $\mathbf{A}$ of $b_1 = 0$. The solution of $e^{\mathbf{A}t}$ of $b_1 = 0$ which can be simplified by Eq. (14) or computed by the calssical method is

$$\mathbf{Exp}(\mathbf{A}_{\mathbf{FID}}) \equiv \begin{bmatrix} e^{-tR_2}\cos(t\omega) & -e^{-tR_2}\sin(t\omega) & 0 & 0 \\ e^{-tR_2}\sin(t\omega) & e^{-tR_2}\cos(t\omega) & 0 & 0 \\ 0 & 0 & e^{-tR_1} & -e^{-tR_1}+1 \\ 0 & 0 & 0 & 1 \end{bmatrix} \tag{B.2}$$

Appendix C. The solution of the case $R_1 = R_2$

When R_1 is equal to R_2, eigenvalues of the matrix $\mathbf{A}$ have tidy expressions,

$$\boldsymbol{\lambda}(\mathbf{A}(R_1 = R_2)) = \begin{bmatrix} -R_2 \\ -R_2 + i\sqrt{\omega^2 + b_1^2} \\ -R_2 - i\sqrt{\omega^2 + b_1^2} \\ 0 \end{bmatrix} \tag{C.1}$$

then, $e^{\lambda_1 t}\mathbf{L}_1(\mathbf{A})$, $e^{\lambda_2 t}\mathbf{L}_2(\mathbf{A}) + e^{\lambda_3 t}\mathbf{L}_3(\mathbf{A})$, and $e^{\lambda_4 t}\mathbf{L}_4(\mathbf{A})$ will be simplified as

$$e^{\lambda_1 t}\mathbf{L}_1(\mathbf{A}) = e^{-tR_2}\begin{bmatrix} \frac{b_1^2(\cos(\phi))^2}{\omega^2+b_1^2} & \frac{b_1^2\sin(\phi)\cos(\phi)}{\omega^2+b_1^2} & \frac{\omega b_1\cos(\phi)}{\omega^2+b_1^2} & -\frac{\omega b_1\cos(\phi)}{\omega^2+b_1^2} \\ \frac{b_1^2\sin(\phi)\cos(\phi)}{\omega^2+b_1^2} & \frac{b_1^2(\sin(\phi))^2}{\omega^2+b_1^2} & \frac{\omega b_1\sin(\phi)}{\omega^2+b_1^2} & -\frac{\omega b_1\sin(\phi)}{\omega^2+b_1^2} \\ \frac{\omega b_1\cos(\phi)}{\omega^2+b_1^2} & \frac{\omega b_1\sin(\phi)}{\omega^2+b_1^2} & \frac{\omega^2}{\omega^2+b_1^2} & -\frac{\omega^2}{\omega^2+b_1^2} \\ 0 & 0 & 0 & 0 \end{bmatrix} \tag{C.2a}$$

$$\left(e^{\lambda_2 t}\mathbf{L}_2(\mathbf{A}) + e^{\lambda_3 t}\mathbf{L}_3(\mathbf{A})\right) = [\mathbf{v_1} \quad \mathbf{v_2} \quad \mathbf{v_3} \quad \mathbf{v_4}] \tag{C.2b}$$

$$e^{\lambda_4 t}\mathbf{L}_4(\mathbf{A}) = \begin{bmatrix} 0 & 0 & 0 & \frac{b_1(\omega\cos(\phi)+\sin(\phi)R_2)}{R_2^2+\omega^2+b_1^2} \\ 0 & 0 & 0 & \frac{b_1(\omega\sin(\phi)-\cos(\phi)R_2)}{R_2^2+\omega^2+b_1^2} \\ 0 & 0 & 0 & \frac{\omega^2+R_2^2}{R_2^2+\omega^2+b_1^2} \\ 0 & 0 & 0 & 1 \end{bmatrix} \tag{C.2c}$$

and

$$\mathbf{v_1} = \begin{bmatrix} -\frac{e^{-tR_2}\left(-b_1^2+b_1^2(\cos(\phi))^2-\omega^2\right)\cos\left(t\sqrt{\omega^2+b_1^2}\right)}{\omega^2+b_1^2} \\ -\frac{b_1^2\sin(\phi)\cos(\phi)e^{-tR_2}\cos\left(t\sqrt{\omega^2+b_1^2}\right)}{\omega^2+b_1^2} + \frac{\sin\left(t\sqrt{\omega^2+b_1^2}\right)\omega e^{-tR_2}}{\sqrt{\omega^2+b_1^2}} \\ -\frac{\omega b_1\cos(\phi)e^{-tR_2}\cos\left(t\sqrt{\omega^2+b_1^2}\right)}{\omega^2+b_1^2} - \frac{\sin\left(t\sqrt{\omega^2+b_1^2}\right)b_1\sin(\phi)e^{-tR_2}}{\sqrt{\omega^2+b_1^2}} \\ 0 \end{bmatrix} \tag{C.3a}$$

$$\mathbf{v_2} = \begin{bmatrix} -\frac{b_1^2\sin(\phi)\cos(\phi)e^{-tR_2}\cos\left(t\sqrt{\omega^2+b_1^2}\right)}{\omega^2+b_1^2} - \frac{\sin\left(t\sqrt{\omega^2+b_1^2}\right)\omega e^{-tR_2}}{\sqrt{\omega^2+b_1^2}} \\ \frac{\left(\omega^2+b_1^2(\cos(\phi))^2\right)e^{-tR_2}\cos\left(t\sqrt{\omega^2+b_1^2}\right)}{\omega^2+b_1^2} \\ -\frac{\omega b_1\sin(\phi)e^{-tR_2}\cos\left(t\sqrt{\omega^2+b_1^2}\right)}{\omega^2+b_1^2} + \frac{\sin\left(t\sqrt{\omega^2+b_1^2}\right)b_1\cos(\phi)e^{-tR_2}}{\sqrt{\omega^2+b_1^2}} \\ 0 \end{bmatrix} \tag{C.3b}$$

$$\mathbf{v_3} = \begin{bmatrix} -\frac{\omega b_1\cos(\phi)e^{-tR_2}\cos\left(t\sqrt{\omega^2+b_1^2}\right)}{\omega^2+b_1^2} + \frac{\sin\left(t\sqrt{\omega^2+b_1^2}\right)b_1\sin(\phi)e^{-tR_2}}{\sqrt{\omega^2+b_1^2}} \\ -\frac{\omega b_1\sin(\phi)e^{-tR_2}\cos\left(t\sqrt{\omega^2+b_1^2}\right)}{\omega^2+b_1^2} - \frac{\sin\left(t\sqrt{\omega^2+b_1^2}\right)b_1\cos(\phi)e^{-tR_2}}{\sqrt{\omega^2+b_1^2}} \\ \frac{b_1^2e^{-tR_2}\cos\left(t\sqrt{\omega^2+b_1^2}\right)}{\omega^2+b_1^2} \\ 0 \end{bmatrix} \tag{C.3c}$$

$$\mathbf{v_4} = e^{-R_2 t}\begin{bmatrix} v_{4,1}+v_{4,2} \\ v_{4,3}+v_{4,4} \\ -\frac{b_1^2 R_2^2 \cos\left(t\sqrt{\omega^2+b_1^2}\right)}{\left(\omega^2+b_1^2\right)\left(R_2^2+\omega^2+b_1^2\right)}+\frac{b_1^2 R_2 \sin\left(t\sqrt{\omega^2+b_1^2}\right)}{\sqrt{\omega^2+b_1^2}\left(R_2^2+\omega^2+b_1^2\right)} \\ 0 \end{bmatrix} \tag{C.3d}$$

with

$$v_{4,1} = -\frac{R_2 b_1\left(\sin(\phi)(\omega^2+b_1^2)-\omega\cos(\phi)R_2\right)\cos\left(t\sqrt{\omega^2+b_1^2}\right)}{\left(\omega^2+b_1^2\right)\left(R_2^2+\omega^2+b_1^2\right)} \tag{C.4a}$$

$$v_{4,2} = -\frac{R_2 b_1\left(\sqrt{\omega^2+b_1^2}\sin(\phi)R_2+\omega\cos(\phi)\sqrt{\omega^2+b_1^2}\right)\sin\left(t\sqrt{\omega^2+b_1^2}\right)}{\left(\omega^2+b_1^2\right)\left(R_2^2+\omega^2+b_1^2\right)} \tag{C.4b}$$

$$v_{4,3} = -\frac{R_2 b_1\left(-\cos(\phi)\left(\omega^2-b_1^2\right)-\omega\sin(\phi)R_2\right)\cos\left(t\sqrt{\omega^2+b_1^2}\right)}{\left(\omega^2+b_1^2\right)\left(R_2^2+\omega^2+b_1^2\right)} \tag{C.4c}$$

$$v_{4,4} = -\frac{R_2 b_1\left(-\sqrt{\omega^2+b_1^2}\cos(\phi)R_2+\omega\sin(\phi)\sqrt{\omega^2+b_1^2}\right)\sin\left(t\sqrt{\omega^2+b_1^2}\right)}{\left(\omega^2+b_1^2\right)\left(R_2^2+\omega^2+b_1^2\right)} \tag{C.4d}$$

The phase cycling scheme $\{\phi, \phi+\pi\}$ of pulses makes the solution of the Bloch equations of $R_1 = R_2$ to be simple which is shown in the following expression:

$$\frac{e^{t\mathbf{A}_\phi}+e^{t\mathbf{A}_{\phi+\pi}}}{2} = \begin{bmatrix} E_{11} & E_{12} & 0 & 0 \\ E_{21} & E_{22} & 0 & 0 \\ 0 & 0 & E_{33} & E_{34} \\ 0 & 0 & 0 & 1 \end{bmatrix} \tag{C.5}$$

and

$$E_{11} = e^{-R_2 t}\left(\frac{b_1^2(\cos(\phi))^2\left(1-\cos\left(t\sqrt{b_1^2+\omega^2}\right)\right)}{b_1^2+\omega^2}+\cos\left(t\sqrt{b_1^2+\omega^2}\right)\right) \tag{C.6a}$$

$$E_{12} = e^{-R_2 t}\left(\frac{b_1^2\sin(\phi)\cos(\phi)\left(1-\cos\left(t\sqrt{b_1^2+\omega^2}\right)\right)}{b_1^2+\omega^2}-\frac{\sin\left(t\sqrt{b_1^2+\omega^2}\right)\omega}{\sqrt{b_1^2+\omega^2}}\right) \tag{C.6b}$$

$$E_{21} = e^{-R_2 t}\left(\frac{b_1^2\sin(\phi)\cos(\phi)\left(1-\cos\left(t\sqrt{b_1^2+\omega^2}\right)\right)}{b_1^2+\omega^2}+\frac{\sin\left(t\sqrt{b_1^2+\omega^2}\right)\omega}{\sqrt{b_1^2+\omega^2}}\right) \tag{C.6c}$$

$$E_{22} = \frac{e^{-R_2 t}\left(b_1^2(\sin(\phi))^2+\cos\left(t\sqrt{b_1^2+\omega^2}\right)\left(\omega^2+b_1^2(\cos(\phi))^2\right)\right)}{b_1^2+\omega^2} \tag{C.6d}$$

$$E_{33} = \frac{e^{-R_2 t}\left(\omega^2+\cos\left(t\sqrt{b_1^2+\omega^2}\right)b_1^2\right)}{b_1^2+\omega^2} \tag{C.6e}$$

$$E_{34} = \frac{E_{34,1}}{E_{34,2}} \tag{C.6f}$$

with

$$E_{34,1} = \left\{\left[\left(\sin\left(t\sqrt{\omega^2+b_1^2}\right)\sqrt{\omega^2+b_1^2}R_2-R_2^2\cos\left(t\sqrt{\omega^2+b_1^2}\right)-\omega^2\right)\times e^{-tR_2}+\omega^2+R_2^2\right]b_1^2+\left(-\omega^4-R_2^2\omega^2\right)e^{-tR_2}+\omega^4+R_2^2\omega^2\right\} \tag{C.7a}$$

$$E_{34,2} = \left\{\left(\omega^2+b_1^2\right)\left(R_2^2+\omega^2+b_1^2\right)\right\} \tag{C.7b}$$

The phase cycling schemes $\{0,\pi\}$ and $\{\frac{\pi}{2},\frac{3\pi}{2}\}$ even give simpler expressions. The above equations show that the decay rate of the transverse magnetization during a soft pulse is R_2, but offsets will affect the amplitude of the magnetizations.

Appendix D. Calculations of the Hahn echo

D.1. The exact solution with phase cycling of model 0

In this subsection, we will give the formula to compute the transverse magnetization with intermediate variables for the Hahn echo with a phase cycle scheme. With these intermediate variables, a constrained optimization problem can be configured to fit the measurement of the transverse relaxation rate.

The effective matrix ($\mathbf{Exp}(\mathbf{A}_{\pi\mathbf{002}})$) of a pulse with phases 0 and π can be written as

$$\mathbf{Exp}(\mathbf{A}_{\pi\mathbf{002}}) = \begin{bmatrix} c_{11}e^{\lambda_1 t_p}+d_{11}e^{u_2 t_p} & c_{12}e^{\lambda_1 t_p}+d_{12}e^{u_2 t_p} & 0 & 0 \\ c_{21}e^{\lambda_1 t_p}+d_{21}e^{u_2 t_p} & c_{22}e^{\lambda_1 t_p}+d_{22}e^{u_2 t_p} & 0 & 0 \\ 0 & 0 & \times & \times \\ 0 & 0 & 0 & 1 \end{bmatrix} \tag{D.1}$$

where $\times$s which are non-zero are not displayed because they are not used in the next computation, c_{11}, c_{12}, c_{21}, c_{22}, d_{11}, d_{12}, d_{21}, d_{22} are corresponding to coefficients of entries with respect to $exp(\lambda_1 t_p)$ and $exp(u_2 t_p)$,

$$c_{11} = -\frac{-3\omega^2 R_2-2\omega^2 u_2+R_2^3+2R_2^2 u_2+R_2 u_2^2+R_2 u_3^2}{\lambda_1\left(\lambda_1^2-2\lambda_1 u_2+u_2^2+u_3^2\right)} \tag{D.2a}$$

$$c_{12} = -\frac{4\omega R_2 u_2+\omega u_2^2+\omega u_3^2+3\omega R_2^2-\omega^3-\omega b_1^2}{\lambda_1\left(\lambda_1^2-2\lambda_1 u_2+u_2^2+u_3^2\right)} \tag{D.2b}$$

$$c_{21} = -c_{12} \tag{D.2c}$$

$$c_{22} = \frac{(2u_2+R_1+2R_2)b_1^2+(3R_2+2u_2)\omega^2-R_2^3-2R_2^2 u_2+\left(-u_2^2-u_3^2\right)R_2}{\lambda_1\left(\lambda_1^2-2\lambda_1 u_2+u_2^2+u_3^2\right)} \tag{D.2d}$$

$$\begin{aligned} d_{11} = {} & \left\{\left\{u_2\left(-\lambda_1 R_2+\omega^2-R_2^2\right)\left(-3u_3^2+u_2^2\right.\right.\right. \\ & \left.+R_2\left(u_2^2-u_3^2\right)\left(3\omega^2-R_2^2+\lambda_1^2\right)+\lambda_1 u_2\left(\left(R_2^2-\omega^2\right)\lambda_1\right. \\ & \left.\left.+R_2\left(R_2^2-3\omega^2\right)\right)\right\}\sin(u_3 t_p)+\{((3u_3\lambda_1-6u_3u_2)R_2 \\ & +u_3\lambda_1^2-3u_2^2u_3+u_3^3)\omega^2+(-u_3\lambda_1+2u_3u_2)R_2^3 \\ & +\left(-u_3\lambda_1^2+3u_2^2u_3-u_3^3\right)R_2^2+\left(-2u_3\lambda_1^2u_2+\left(3u_2^2u_3-u_3^3\right)\lambda_1\right)R_2\} \\ & \times\cos(u_3 t_p)\}/\left\{u_3\left(u_2^2+u_3^2\right)\left((\lambda_1-u_2)^2+u_3^2\right)\right\} \end{aligned} \tag{D.2e}$$

$$d_{12} = \Big\{\Big\{\omega\Big((-\lambda_1 u_2 - u_3^2 + u_2^2)\Big(\omega^2 + b_1^2 - 3R_2^2\Big) + 2u_2R_2(3u_3^2 - u_2^2 + \lambda_1^2) + \lambda_1 u_3^2(3u_2 - \lambda_1) + \lambda_1 u_2^2(\lambda_1 - u_2)\Big)\Big\}\sin(u_3 t_p) + \Big\{-u_3\omega\Big(\Big(\omega^2 + b_1^2 - 3R_2^2\Big)(2u_2 - \lambda_1) + 2R_2(u_3^2 - 3u_2^2 + \lambda_1^2) + \lambda_1(u_3^2 + 2\lambda_1 u_2 - 3u_2^2)\Big)\Big\} \times \cos(u_3 t_p)\Big\}/\Big\{u_3(u_2^2 + u_3^2)\Big((\lambda_1 - u_2)^2 + u_3^2\Big)\Big\} \tag{D.2f}$$

$$d_{21} = -d_{12} \tag{D.2g}$$

$$d_{22} = \Big\{\Big\{\big((2u_2^2 - 2u_3^2 - 2\lambda_1 u_2)R_2 + (-R_1 - 3u_2)u_3^2 + u_2^3 + R_1 u_2^2 + (-\lambda_1^2 - R_1\lambda_1)u_2\big)b_1^2 + \big((-3\lambda_1 u_2 + 3u_2^2 - 3u_3^2)R_2 + u_3^2 - \lambda_1^2 u_2 - 3u_3^2 u_2\big)\omega^2 + \big(-u_2^2 + \lambda_1 u_2 + u_3^2\big)R_2^2 + \big(-u_2^3 + \lambda_1^2 u_2 + 3u_3^2 u_2\big)R_2^2 + \big((3\lambda_1 u_2 - \lambda_1^2)u_3^2 + \lambda_1^2 u_2^2 - \lambda_1 u_2^3\big)R_2\Big\} \times \sin(u_3 t_p) + u_3\Big\{\big((-4u_2 + 2\lambda_1)R_2 + u_3^2 + \lambda_1^2 + R_1\lambda_1 - 3u_2^2 - 2R_1 u_2\big)b_1^2 + \big((3\lambda_1 - 6u_2)R_2 + u_3^2 - 3u_2^2 + \lambda_1^2\big)\omega^2 + \Big(2u_2 - \lambda_1\Big)R_2^3 + \big(-u_3^2 - \lambda_1^2 + 3u_2^2\big)R_2^2 + \big(3\lambda_1 u_2^2 - 2\lambda_1^2 u_2 - u_3^2\lambda_1\big)R_2\Big\} \times \cos(u_3 t_p)\Big\}/\Big\{u_3(u_2^2 + u_3^2)\Big((\lambda_1 - u_2)^2 + u_3^2\Big)\Big\} \tag{D.2h}$$

Then according to Eqs. (25), (B.2) and (D.1), the transverse magnetizations are

$$M_{x,j} = \Big\{-\big(c_{22}e^{\lambda_1 t_p} + d_{22}e^{u_2 t_p}\big)(\sin(\tau_j\omega))^2 + \big(2c_{12}e^{\lambda_1 t_p} + 2d_{12}e^{u_2 t_p}\big) \times \cos\Big(\tau_j\omega)\sin(\tau_j\omega) + \big(c_{11}e^{\lambda_1 t_p} + d_{11}e^{u_2 t_p}\big)(\cos(\tau_j\omega))^2\Big\}e^{-2R_2\tau_j} \tag{D.3a}$$

$$M_{y,j} = \Big\{\big(c_{12}e^{\lambda_1 t_p} + d_{12}e^{u_2 t_p}\big)(\sin(\tau_j\omega))^2 + \big(c_{11}e^{\lambda_1 t_p} + d_{11}e^{u_2 t_p} + c_{22}e^{\lambda_1 t_p} + d_{22}e^{u_2 t_p}\big)\cos(\tau_j\omega)\sin(\tau_j\omega) + \Big(\cos(\tau_j\omega)^2\big(-c_{12}e^{\lambda_1 t_p} - d_{12}e^{u_2 t_p}\big)\Big\}e^{-2R_2\tau_j} \tag{D.3b}$$

where τ_j is the jth delay time of a series of Hahn echo experiments.

D.2. The solutions of model 2

This subsection displays expressions of the transverse magnetization which are approximated by Model 2 with different phases.

The transverse magnetizations after the pulse sequence $\frac{\pi}{2y} - \tau - \frac{\pi}{2\pm x} - t_p - \frac{\pi}{2\pm x} - \tau -$ are

$$M_{x,j} = e^{-2\tau_j R_2}\Big(e^{-t_p R_2}(\cos(\tau_j\omega))^2\cos(t_p\omega) + e^{-t_p R_1}(\sin(\tau_j\omega))^2\Big) \tag{D.4a}$$

$$M_{y,j} = e^{-2\tau_j R_2}\cos(\tau_j\omega)\sin(\tau_j\omega)(e^{-t_p R_2}\cos(t_p\omega) - e^{-t_p R_1}) \tag{D.4b}$$

The transverse magnetizations after the pulse sequence $\frac{\pi}{2y} - \tau - \frac{\pi}{2x} - t_p - \frac{\pi}{2x} - \tau -$ are

$$M_{x,j} = -e^{-\tau_j R_2}(-e^{-(\tau_j + t_p)R_2}(\cos(\tau_j\omega))^2\cos(t_p\omega) - e^{-\tau_j R_2 - t_p R_1}(\sin(\tau_j\omega))^2 + \cos(\tau_j\omega)e^{-t_p R_2}\sin(t_p\omega)(e^{-\tau_j R_1} - 1) + \sin(\tau_j\omega)(-1 + e^{-t_p R_1})) \tag{D.5a}$$

$$M_{y,j} = -e^{-\tau_j R_2}(\cos(\tau_j\omega)\sin(\tau_j\omega)e^{-\tau_j R_2}(-e^{-t_p R_2}\cos(t_p\omega) + e^{-t_p R_1}) + \sin(\tau_j\omega)\sin(t_p\omega)e^{-t_p R_2}(e^{-\tau_j R_1} - 1) + \cos(\tau_j\omega)(1 - e^{-t_p R_1})) \tag{D.5b}$$

The transverse magnetizations after the pulse sequence $\frac{\pi}{2y} - \tau - \frac{\pi}{2y} - t_p - \frac{\pi}{2y} - \tau -$ are

$$M_{x,j} = e^{-\tau_j R_2}(-e^{-(\tau_j + t_p)R_2}\cos(t_p\omega)(\sin(\tau_j\omega))^2 - e^{-\tau_j R_2 - t_p R_1}(\cos(\tau_j\omega))^2 + \sin(\tau_j\omega)\sin(t_p\omega)e^{-t_p R_2}(e^{-\tau_j R_1} - 1) + \cos(\tau_j\omega)(1 - e^{-t_p R_1})) \tag{D.6a}$$

$$M_{y,j} = -e^{-\tau_j R_2}(\cos(\tau_j\omega)\sin(\tau_j\omega)e^{-\tau_j R_2}(-e^{-t_p R_2}\cos(t_p\omega) + e^{-t_p R_1}) + \cos(\tau_j\omega)e^{-t_p R_2}\sin(t_p\omega)(e^{-\tau_j R_1} - 1) + \sin(\tau_j\omega)(-1 + e^{-t_p R_1})) \tag{D.6b}$$

The fitting models of using Model 2 approximation for different phases and the phase cycling can be obtained by replacing $M_{x,j}$ and $M_{y,j}$ into the optimization problem (28).

D.3. The solutions of model 3

The effective matrix of Model 3 is calculated by

$$\mathbf{Exp}(\mathbf{A}_\pi) = \mathbf{Exp}(\mathbf{A_{Relax3}}) \cdot \mathbf{Exp}(\mathbf{A}_{\pi 3}) \cdot \mathbf{Exp}(\mathbf{A_{Relax3}}) \tag{D.7}$$

where $\mathbf{Exp}(\mathbf{A_{Relax3}})$ represents the relax matrix of on-resonance, $\mathbf{Exp}(\mathbf{A}_{\pi\mathbf{3}})$ represents the general effective matrix of the pulse without the relaxation,

$$\mathbf{Exp}(\mathbf{A_{Relax3}}) = \begin{bmatrix} e^{-1/2t_p R_2} & 0 & 0 & 0 \\ 0 & e^{-1/2t_p R_2} & 0 & 0 \\ 0 & 0 & e^{-1/2t_p R_1} & -e^{-1/2t_p R_1} + 1 \\ 0 & 0 & 0 & 1 \end{bmatrix} \tag{D.8}$$

$$\mathbf{Exp}(\mathbf{A}_{\pi\mathbf{3}}) = \begin{bmatrix} P_{11} & P_{12} & P_{13} & 0 \\ P_{21} & P_{22} & P_{23} & 0 \\ P_{31} & P_{32} & P_{33} & 0 \\ 0 & 0 & 0 & 1 \end{bmatrix} \tag{D.9}$$

where $P_{11}, P_{12}, P_{13}, P_{21}, P_{22}, P_{23}, P_{31}, P_{32}, P_{33}$ are elements of the matrix $\mathbf{Exp}(\mathbf{A}_{\pi\mathbf{3}})$.

Thus, the general expressions of the transverse magnetization computed by Model 3 approximation are

$$M_{x,j} = e^{-1/2R_2(2\tau_j + t_p)}(e^{-1/2R_2(2\tau_j + t_p)}\cos(\tau_j\omega)(\cos(\tau_j\omega)P_{11} + \sin(\tau_j\omega)(P_{12} - P_{21})) + -e^{-1/2R_2(2\tau_j + t_p)}P_{22}(\sin(\tau_j\omega))^2 + \cos(\tau_j\omega)P_{13} - \sin(\tau_j\omega)P_{23} + e^{-1/2R_1(2\tau_i + t_p)}(-\cos(\tau_j\omega)P_{13} + \sin(\tau_j\omega)P_{23})) \tag{D.10a}$$

$$M_{y,j} = e^{-1/2R_2(2\tau_j + t_p)}(e^{-1/2R_2(2\tau_j + t_p)}(\cos(\tau_i\omega)(\sin(\tau_j\omega)(P_{11} + P_{22}) + \cos(\tau_j\omega)P_{21}) + P_{12}(\sin(\tau_j\omega))^2) + e^{-1/2R_1(2\tau_j + t_p)}(-\sin(\tau_i\omega)P_{13} - \cos(\tau_j\omega)P_{23}) + \sin(\tau_j\omega)P_{13} + \cos(\tau_j\omega)P_{23}) \tag{D.10b}$$

The specific expressions for different phases of the echo pulse or the phase cycling can be obtained by substituting the matrix $\mathbf{Exp}(\mathbf{A}_{\pi\mathbf{3}})$ which are demonstrated in the following.

The effective matrix of the pulse with the phase scheme of phases $\{0, \pi\}$ when the relaxation is ignored is

$$\mathbf{Exp}(\mathbf{A}_{\pi\mathbf{302}})=\begin{bmatrix}\frac{b_1^2+\omega^2\cos\left(\sqrt{b_1^2+\omega^2}t_p\right)}{b_1^2+\omega^2} & -\frac{\omega\sin\left(\sqrt{b_1^2+\omega^2}t_p\right)}{\sqrt{b_1^2+\omega^2}} & 0 & 0\\ \frac{\omega\sin\left(\sqrt{b_1^2+\omega^2}t_p\right)}{\sqrt{b_1^2+\omega^2}} & \cos\left(\sqrt{b_1^2+\omega^2}t_p\right) & 0 & 0\\ 0 & 0 & \frac{\omega^2+b_1^2\cos\left(\sqrt{b_1^2+\omega^2}t_p\right)}{b_1^2+\omega^2} & 0\\ 0 & 0 & 0 & 1\end{bmatrix} \tag{D.11}$$

which can be directly computed by setting R_1,R_2 to be 0 in the matrix **A**. Subsitituting $\mathbf{Exp}(\mathbf{A}_{\pi\mathbf{3}})$ with $\mathbf{Exp}(\mathbf{A}_{\pi\mathbf{302}})$, the transverse magnetizations for this approximation are

$$M_{xj}=\left(-\frac{\omega\sin\left(\sqrt{b_1^2+\omega^2}t_p\right)\sin(2\tau_j\omega)}{\sqrt{b_1^2+\omega^2}}+\frac{b_1^2(\cos(\tau_j\omega))^2}{b_1^2+\omega^2}+\frac{(\omega^2\cos(2\tau_j\omega)-b_1^2(\sin(\tau_j\omega))^2)\cos\left(\sqrt{b_1^2+\omega^2}t_p\right)}{b_1^2+\omega^2}\right)e^{-R_2(2\tau_j+t_p)} \tag{D.12a}$$

$$M_{yj}=\left(1/2\left(\frac{\left(2\omega^2+b_1^2\right)\cos\left(\sqrt{b_1^2+\omega^2}t_p\right)}{b_1^2+\omega^2}+\frac{b_1^2}{b_1^2+\omega^2}\right)\sin(2\tau_j\omega)+\frac{\omega\cos(2\tau_j\omega)\sin\left(\sqrt{b_1^2+\omega^2}t_p\right)}{\sqrt{b_1^2+\omega^2}}\right)e^{-R_2(2\tau_j+t_p)} \tag{D.12b}$$

The expressions of the transverse magnetization (Eq. (D.12)) are much simpler than the full solution of the Bloch equations, and they provide good performance when $\|\omega\|\leqslant\gamma B_1$ or $R_1\approx R_2$. This tells us that when $\|\omega\|\leqslant\gamma B_1$, the transverse decay rate during a soft echo pulse is approximate to the true R_2, but the major factor which results in errors of the measurement of R_2 is from offsets which affect the amplitude of the exponential decay. The fitting optimization problem constructed by Eq. (D.12) does not rely on the value of R_1, which means that it is not necessary to obtain the value of R_1 before fitting R_2 if the phase cycling is applied.

The effective matrix of the soft echo pulse when it is along with the x axis and the relaxation is ignored is

$$\mathbf{Exp}(\mathbf{A}_{\pi\mathbf{30}})=\begin{bmatrix}\frac{b_1^2+\omega^2\cos\left(\sqrt{b_1^2+\omega^2}t_p\right)}{b_1^2+\omega^2} & -\frac{\omega\sin\left(\sqrt{b_1^2+\omega^2}t_p\right)}{\sqrt{b_1^2+\omega^2}} & -\frac{b_1\omega\left(\cos\left(\sqrt{b_1^2+\omega^2}t_p\right)-1\right)}{b_1^2+\omega^2} & 0\\ \frac{\omega\sin\left(\sqrt{b_1^2+\omega^2}t_p\right)}{\sqrt{b_1^2+\omega^2}} & \cos\left(\sqrt{b_1^2+\omega^2}t_p\right) & -\frac{\sin\left(\sqrt{b_1^2+\omega^2}t_p\right)b_1}{\sqrt{b_1^2+\omega^2}} & 0\\ -\frac{b_1\omega\left(\cos\left(\sqrt{b_1^2+\omega^2}t_p\right)-1\right)}{b_1^2+\omega^2} & \frac{\sin\left(\sqrt{b_1^2+\omega^2}t_p\right)b_1}{\sqrt{b_1^2+\omega^2}} & \frac{\omega^2+b_1^2\cos\left(\sqrt{b_1^2+\omega^2}t_p\right)}{b_1^2+\omega^2} & 0\\ 0 & 0 & 0 & 1\end{bmatrix} \tag{D.13}$$

The effective matrix of the pulse with the phase $\frac{\pi}{2}$ when the relaxation is ignored is

$$\mathbf{Exp}(\mathbf{A}_{\pi\mathbf{31}})=\begin{bmatrix}\cos\left(\sqrt{b_1^2+\omega^2}t_p\right) & -\frac{\omega\sin\left(\sqrt{b_1^2+\omega^2}t_p\right)}{\sqrt{b_1^2+\omega^2}} & \frac{\sin\left(\sqrt{b_1^2+\omega^2}t_p\right)b_1}{\sqrt{b_1^2+\omega^2}} & 0\\ \frac{\omega\sin\left(\sqrt{b_1^2+\omega^2}t_p\right)}{\sqrt{b_1^2+\omega^2}} & \frac{b_1^2+\omega^2\cos\left(\sqrt{b_1^2+\omega^2}t_p\right)}{b_1^2+\omega^2} & -\frac{b_1\omega\left(\cos\left(\sqrt{b_1^2+\omega^2}t_p\right)-1\right)}{b_1^2+\omega^2} & 0\\ -\frac{\sin\left(\sqrt{b_1^2+\omega^2}t_p\right)b_1}{\sqrt{b_1^2+\omega^2}} & -\frac{b_1\omega\left(\cos\left(\sqrt{b_1^2+\omega^2}t_p\right)-1\right)}{b_1^2+\omega^2} & \frac{\omega^2+b_1^2\cos\left(\sqrt{b_1^2+\omega^2}t_p\right)}{b_1^2+\omega^2} & 0\\ 0 & 0 & 0 & 1\end{bmatrix} \tag{D.14}$$

Respectively substituting $\mathbf{Exp}(\mathbf{A}_{\pi\mathbf{3}})$ with $\mathbf{Exp}(\mathbf{A}_{\pi\mathbf{30}})$ and $\mathbf{Exp}(\mathbf{A}_{\pi\mathbf{31}})$ into Eq. (D.7), the magnetization before the acquisition for phases 0 and $\pi/2$ of the echo pulse can be achieved. Clearly, if ω is not equal to 0, the entries P_{13} and P_{23} will not be zero in these two cases, this means that the z magnetization will affect the transverse magnetization. Thus, the fitting models constructed for these phases require that R_1 is known.

D.4. The solutions of model 4

The effective matrix of Model 4 is calculated by

$$\mathbf{Exp}(\mathbf{A}_{\pi})=\mathbf{Exp}(\mathbf{A}_{\pi\mathbf{4}}).\mathbf{Exp}(\mathbf{A}_{\mathbf{Relax4}}).\mathbf{Exp}(\mathbf{A}_{\pi\mathbf{4}}) \tag{D.15}$$

where $\mathbf{Exp}(\mathbf{A}_{\pi\mathbf{4}})$ is obtained by substituting t_p of Eqs. (D.11), (D.13) or (D.14) with $t_p/2$, and $\mathbf{Exp}(\mathbf{A}_{\mathbf{Relax}4})$ is obtained by substituting t_p of Eq. (D.8) with $2t_p$, then the transverse magnetization for this approximation of Model 4 with respect to the phase cycling, phase 0 and $\pi/2$ is calculated by Eq. (25) (results are not shown).

References

[1] R.R. Ernst, G. Bodenhausen, A. Wokaun, Principles of Nuclear Magnetic Resonance in One and Two Dimensions, Clarendon Press, Oxford, 1987.
[2] M.H. Levitt, Spin Dynamics: Basics of Nuclear Magnetic Resonance, John Wiley & Sons, Chichester; New York, 2001.
[3] J. Keeler, Understanding NMR Spectroscopy, John Wiley & Sons, Chichester; Hoboken, NJ, 2005.
[4] P.-O. Löwdin, The normal constants of motion in quantum mechanics treated by projection technique, Rev. Mod. Phys. 34 (1962) 520–530.
[5] N. Chandrakumar, Application of Löwdin projectors to evaluate density matrix evolutions, J. Magn. Reson. 88 (1990) 86–92.
[6] F. Bloch, W.W. Hansen, M. Packard, Nuclear induction, Phys. Rev. 69 (1946) 127.
[7] F. Bloch, Nuclear induction, Phys. Rev. 70 (1946) 460–474.
[8] J.A. Pople, High-Resolution Nuclear Magnetic Resonance, McGraw-Hill, New York, 1959.
[9] A. Carrington, A.D. McLachlan, Introduction to Magnetic Resonance with Applications to Chemistry and Chemical Physics, Harper & Row, New York, 1967.
[10] E.M. Haacke, R.W. Brown, M.R. Thompson, R. Venkatesan, Magnetic Resonance Imaging: Physical Principles and Sequence Design, Wiley-Liss, New York, 1999.
[11] H.C. Torrey, Transient nutations in nuclear magnetic resonance, Phys. Rev. 76 (1949) 1059–1068.
[12] G.A. Morris, P.B. Chilvers, General analytical solutions of the Bloch equations, J. Magn. Reson. Ser. A 107 (1994) 236–238.
[13] G.A. Morris, P.B. Chilvers, Erratum: volume 107, number 2, series A (1994) in the note, "General Analytical Solutions of the Bloch Equations," by Gareth A. Morris and Paul B. Chilvers, pages 236-238, J. Magn. Reson. Ser. A 111 (1994b) 232–232.
[14] P.K. Madhu, A. Kumar, Direct Cartesian-space solutions of generalized Bloch equations in the rotating frame, J. Magn. Reson. Ser. A 114 (1995) 201–211.
[15] P.K. Madhu, A. Kumar, Bloch equations revisited: new analytical solutions for the generalized Bloch equations, Concepts Magn. Reson. 9 (1997) 1–12.
[16] K.J. Packer, K.M. Wright, The use of single-spin operator basis sets in the N.M.R. spectroscopy of scalar-coupled spin systems, Mol. Phys. 50 (1983) 797–813.
[17] O.W. Sorensen, G.W. Eich, M.H. Levitt, G. Bodenhausen, R.R. Ernst, Product operator formalism for the description of NMR pulse experiments, Prog. Nucl. Magn. Reson. Spectrosc. 16 (1984) 163–192.
[18] G.N.B. Yip, E.R.P. Zuiderweg, A phase cycle scheme that significantly suppresses offset-dependent artifacts in the R_2-CPMG ^{15}N relaxation experiment, J. Magn. Reson. 171 (2004) 25–36.
[19] N.I. Gershenzon, K. Kobzar, B. Luy, S.J. Glaser, T.E. Skinner, Optimal control design of excitation pulses that accommodate relaxation, J. Magn. Reson. 188 (2007) 330–336.
[20] P. Meakin, J.P. Jesson, Computer simulation of multipulse and Fourier transform NMR experiments. II. Some simulations using the density matrix equation of motion, J. Magn. Reson. 11 (1973) 182–206.
[21] D.D. Traficante, M.M. McGregor, Simple laboratory experiments to observe the manifestations of the Sinc function, Concepts in Magnetic Resonance 14 (2002) 308–325.
[22] W.S. Warren, Effects of arbitrary laser or NMR pulse shapes on population inversion and coherence, The Journal of Chemical Physics 81 (1984) 5437–5448.
[23] R.M. Gregory, A.D. Bain, The effects of finite rectangular pulses in NMR: phase and intensity distortions for a Spin-1/2, Concepts in Magnetic Resonance Part A 34 (2009) 305–314.
[24] M.H. Levitt, Composite pulses, Prog. Nucl. Magn. Reson. Spectrosc. 18 (1986) 61–122.
[25] R. Freeman, Shaped radiofrequency pulses in high resolution NMR, Prog. Nucl. Magn. Reson. Spectrosc. 32 (1998) 59–106.
[26] T.E. Skinner, T.O. Reiss, B. Luy, N. Khaneja, S. Glaser, Application of optimal control theory to the design of broadband excitation pulses for high-resolution NMR, J. Magn. Reson. 163 (2003) 8–15.

[27] T.E. Skinner, T.O. Reiss, B. Luy, N. Khaneja, S.J. Glaser, Reducing the duration of broadband excitation pulses using optimal control with limited RF amplitude, J. Magn. Reson. 167 (2004) 68–74.
[28] K. Kobzar, T.E. Skinner, N. Khaneja, S.J. Glaser, B. Luy, Exploring the limits of broadband excitation and inversion pulses, J. Magn. Reson. 170 (2004) 236–243.
[29] T.E. Skinner, K. Kobzar, B. Luy, M.R. Bendall, W. Bermel, N. Khaneja, S.J. Glaser, Optimal control design of constant amplitude phase-modulated pulses: application to calibration-free broadband excitation, J. Magn. Reson. 179 (2006) 241–249.
[30] C.K. Anand, A.D. Bain, Z. Nie, Simulation of steady-state NMR of coupled systems using Liouville space and computer algebra methods, J. Magn. Reson. 189 (2007) 200–208.
[31] J. Jeener, Superoperators in magnetic resonance, Adv. Magn. Reson. 10 (1982) 1–51.
[32] P. Allard, M. Helgstrand, T. Härd, The complete homogeneous master equation for a heteronuclear two-spin system in the basis of cartesian product operators, J. Magn. Reson. 134 (1998) 7–16.
[33] W. Magnus, On the exponential solution of differential equations for a linear operator, Commun. Pure Appl. Math. 7 (1954) 649–673.
[34] C. Moler, C. Van Loan, Nineteen dubious ways to compute the exponential of a matrix, twenty-five years later, SIAM Rev. 45 (2003) 3–49.
[35] W.A. Harris Jr., J.P. Fillmore, D.R. Smith, Matrix exponentials: another approach, SIAM Rev. 43 (2001) 694–706.
[36] E.P. Fulmer, Computation of the matrix exponential, Am. Math. Mon. 82 (1975) 156–159.
[37] T.M. Apostol, Some explicit formulas for the exponential matrix e^{tA}, Am. Math. Mon. 76 (1969) 289–292.
[38] G. Binsch, Unified theory of exchange effects on nuclear magnetic resonance line shapes, J. Am. Chem. Soc. 91 (1969) 1304–1309.
[39] A.D. Bain, G.J. Duns, A unified approach to dynamic NMR based on a physical interpretation of the transition probability, Can. J. Chem. 74 (1996) 819–824.
[40] A.D. Bain, Chemical exchange in NMR, Prog. Nucl. Magn. Reson. Spectrosc. 43 (2003) 63–103.
[41] R.W.D. Nickalls, A new approach to solving the cubic: Cardan's solution revealed, Math. Gazette 77 (1993) 354–359.
[42] J.H. Wilkinson, The Algebraic Eigenvalue Problem, Clarendon Press, Oxford, 1965.
[43] C.K. Anand, A.D. Bain, Z. Nie, The simulation and optimization of pulsed NMR experiments using a Liouville space method, in: The Proceedings of The Maple Conference, Waterloo, Canada, 2006, pp. 203–216.
[44] G.B. Furman, A.M. Panich, S.D. Goren, Spin-locking in one pulse NMR experiment, Solid State Nucl. Magn. Reson. 11 (1998) 225–230.
[45] D.E. Rourke, A.A. Karabanov, G.H. Booth, I. Frantsuzov, The Bloch Equations when $T_1 = T_2$, Inverse Probl. 23 (2007) 609–623.
[46] F. Massi, E. Johnson, C. Wang, M. Rance, A.G. Palmer, NMR $R_{1\rho}$ rotating-frame relaxation with weak radio frequency fields, J. Am. Chem. Soc. 126 (2004) 2247–2256.
[47] A.J. Wheaton, A. Borthakur, M.T. Corbo, G. Moonis, E. Melhem, R. Reddy, $T_{2\rho}$-weighted contrast in MR images of the human brain, Magn. Reson. Med. 52 (2004) 1223–1227.
[48] L. Eno, On the use of the second order split-operator method, J. Chem. Phys. 113 (2000) 453–454.
[49] M. Suzuki, Decomposition formulas of exponential operators and lie exponentials with some applications to quantum mechanics and statistical physics, J. Math. Phys. 26 (1985) 601–612.
[50] E.L. Hahn, Spin echoes, Phys. Rev. 80 (1950) 580–594.
[51] R.L. Vold, R.R. Vold, H.E. Simon, Errors in measurements of transverse relaxation rates, J. Magn. Reson. 11 (1973) 283–298.
[52] D.G. Hughes, Errors in T_2 values measured with the Carr–Purcell–Meiboom–Gill pulsed NMR sequence, J. Magn. Reson. 26 (1977) 481–489.
[53] E.O. Stejskal, J. Schaefer, Comparisons of quadrature and single-phase fourier transform NMR, J. Magn. Reson. 14 (1974) 160–169.
[54] A.D. Bain, Coherence levels and coherence pathways in NMR: a simple way to design phase cycling procedures, J. Magn. Reson. 56 (1984) 418–427.
[55] S. Meiboom, D. Gill, Modified spin-echo method for measuring nuclear relaxation times, Rev. Sci. Instrum. 29 (1958) 688–691.
[56] H.Y. Carr, E.M. Purcell, Effects of diffusion on free precession in nuclear magnetic resonance experiments, Phys. Rev. 94 (1954) 630–638.
[57] D.M. Korzhnev, E.V. Tischenko, A.S. Arseniev, Off-resonance effects in ^{15}N T_2 CPMG measurements, J. Biomol. NMR 17 (2000) 231–237.
[58] A. Ross, M. Czisch, G.C. King, Systematic errors associated with the CPMG pulse sequence and their effect on motional analysis of biomolecules, J. Magn. Reson. 124 (1997) 355–365.
[59] M. Czisch, G.C. King, A. Ross, Removal of systematic errors associated with off-resonance oscillations in T_2 measurements, J. Magn. Reson. 126 (1997) 154–157.
[60] D. Long, M. Liu, D. Yang, Accurately probing slow motions on millisecond timescales with a robust NMR relaxation experiment, J. Am. Chem. Soc. 130 (2008) 2432–2433.
[61] T.E. Bull, Effect of RF field inhomogeneities on spin-echo measurements, Rev. Sci. Instrum. 45 (1974) 232–242.
[62] S. Mattila, Measurement and Minimization of Field Inhomogeneities in High Resolution NMR, University of Oulu, Oulu, Finland, 2001.
[63] R. Fourer, D.M. Gay, B.W. Kernighan, A modeling language for mathematical programming, Manage. Sci. 36 (1990) 519–554.
[64] A. Wächter, L.T. Biegler, On the implementation of an interior-point filter line-search algorithm for large-scale nonlinear programming, Math. Programm. 106 (2006) 25–57.